/N 34

L ... b

p - 44

ICASE

ON THE MODULATIONAL INSTABILITY OF LARGE AMPLITUDE WAVES IN SUPERSONIC BOUNDARY LAYERS

Philip Hall
Demetrios T. Papageorgiou

On the modulational instability of large amplitude waves in supersonic boundary layers

Philip Hall, Department of Mathematics,
Manchester University, Manchester M13 9PL, UK
and
Demetrios T. Papageorgiou, Department of Mathematics and
Center for Applied Mathematics and Statistics
New Jersey Institute of Technology, Newark, New Jersey 07102, USA

Abstract

The evolution of large amplitude Tollmien-Schlichting waves in a supersonic boundary layer is investigated. Disturbances which have their wavenumber and frequency slowly varying in time and space are described using a phase equation type of approach. Unlike the incompressible case we find that the initial bifurcation to a finite amplitude Tollmien-Schlichting wave is subcritical for most Mach numbers. In fact the bifurcation is only supercritical for a small range of Mach numbers and even then for only a finite range of wave propagation angles. The modulational instability of large amplitude wavetrains is considered and is shown to be governed by an equation similar to Burgers equation but with the viscous term replaced by a fractional derivative. A numerical investigation of the solution of this equation is described. It is shown that uniform wavetrains are unstable.

1 Introduction and triple-deck theory for compressible flows

Consider the flow of a viscous compressible fluid which has pressure, density and speed p_∞^*, ρ_∞^* and u_∞^* sufficiently far away from the semi-infinite plate defined by $y = 0$, $x \geq 0$ with respect to a Cartesian coordinate system made dimensionless using the reference length L. If the viscosity in the free stream is ν_∞^* then we define a Reynolds number R by writing

$$R = \frac{U_\infty^* L}{\nu_\infty^*}, \tag{1}$$

and throughout our investigation we assume $R >> 1$. We scale the velocity and temperature of the flow near the wall on their free stream values and we assume a linear viscosity temperature law which we write in the form

$$\frac{\mu^*}{T^*} = \frac{C \mu_\infty^*}{T_\infty^*} = \left(\frac{\mu_w^*}{T_w^*} \right), \tag{2}$$

where μ^* and T^* are the viscosity and temperature whilst a subscript w denotes a quantity evaluated at the wall. The basic boundary layer flow has smooth velocity temperature and density profiles (Stewartson [16]) and may be calculated routinely. Here we concern ourselves with the large amplitude waves (induced by viscosity) which are known to occur in such flows. A linear theory of Tollmien-Schlichting waves based on triple-deck theory was first given by Smith [13] for incompressible flows. Subsequently Smith [15] developed a linear stability for compressible flows and our concern here is with the development of these Tollmien-Schlichting waves in a strongly nonlinear regime.

In order to describe the nonlinear evolution of Tollmien-Schlichting waves in a compressible boundary layer we use triple-deck theory based on the work of Stewartson and Williams [18] and Stewartson [16]. We introduce the small parameter ϵ defined by

$$\epsilon = R^{-1/8} \tag{3}$$

and look for a solution of the Navier Stokes equations for $\epsilon << 1$.

Suppose that (x, y, z) and (u, v, w) are dimensionless coordinates and velocities scaled on L and u_∞^* respectively. In the triple-deck limit the flow responds on a short $0(\epsilon^3)$ lengthscale in the x direction and the lower deck must be taken to be of order ϵ^5 if viscous and convective terms are to balance. The main deck is simply the region occupied by the undisturbed boundary layer so that $y = 0(\epsilon^4)$ there. Finally the upper deck, where the flow is a potential one, is defined by $y = 0(\epsilon^3)$. Since the streamwise lengthscale is small we must confine our attention to some neighbourhood around the position where instability first occurs. If this position corresponds to $x = \bar{x}$ then we define triple-deck variables X and Z by writing

$$\frac{[x - \bar{x}]}{J \epsilon^3} = X, \quad \frac{z}{J \epsilon^3} = Z, \tag{4a}$$

where

$$J = \frac{C^{3/8} (T_w^*/T_\infty^*)^{3/2}}{(M_\infty^2 - 1)^{3/8} \lambda^{5/4}}. \tag{4b}$$

1

Here J is an $0(1)$ quantity and M_∞ is the free stream Mach number and λ is the unperturbed skin friction at $x = \bar{x}$. The variable Y is $0(1)$ in the lower deck and defined by

$$Y = \frac{y\lambda^{3/4}(M_\infty^2 - 1)^{1/8}}{\epsilon^5 C^{5/8}(T_w^*/T_\infty^*)^{3/2}}. \tag{5}$$

In the main and upper decks the dimensionless variables $\grave{Y}, \overline{Y}$ are defined by

$$\grave{Y} = \frac{y}{\epsilon^4 C^{1/2}(T_w^*/T_w^*)}, \tag{6a}$$

$$\overline{Y} = \frac{y\lambda^{5/4}(M_\infty^* - 1)^{7/8}}{\epsilon^3 C^{3/8}(T_w^*/T_\infty^*)^{3/2}}, \tag{6b}$$

respectively. Note here that the $0(1)$ scaling factors have been introduced in order to simplify the form of the triple-deck equations which we are now in a position to write down.

Lower Deck Equations

Here $u, v, w, p - p_\infty$ expand as

$$u = \epsilon C^{1/8}(T_w^*/T_\infty^*)^{1/2}\lambda^{1/4}(M_\infty^2 - 1)^{-1/8}U + 0(\epsilon^2),$$

$$v = \epsilon^3 C^{3/8}(T_w^*/T_\infty^*)^{1/2}\lambda^{3/4}(M_\infty^2 - 1)^{1/8}V + 0(\epsilon^4),$$

$$w = \epsilon C^{1/8}(T_w^*/T_\infty^*)^{1/2}\lambda^{1/4}(M_\infty^2 - 1)^{-1/8}W + 0(\epsilon^2),$$

$$p - p_\infty = \epsilon^2 C^{1/4}\lambda^{1/2}(M_\infty^2 - 1)^{-1/4}P + 0(\epsilon^3).$$

If we define a dimensionless time variable t by

$$t = \frac{t^* u_\infty^*(M_\infty^2 - 1)^{1/4}\lambda^{3/2}}{L\epsilon^2(T_w^*/T_\infty^*)C^{1/4}}$$

then the zeroth order approximation to the Navier Stokes equations in the lower deck yields

$$\begin{cases} U_X + V_Y + W_Z = 0, \\ U_t + UU_X + VU_Y + WU_Z = -P_X + U_{YY}, \\ W_t + UW_X + VW_Y + WW_Z = -P_Z + W_{YY}, \\ P_Y = 0. \end{cases} \tag{7}$$

Thus the flow is determined by the 3D unsteady boundary layer equations in the lower deck. Note also that the energy equation plays no role in the lower deck since the temperature and density are uniform there, see for example Stewartson and Williams (1969) for a discussion of this point.

At the wall we impose the condition

$$U = V = W = 0, \quad Y = 0, \tag{8}$$

whilst at the edge of the lower deck

$$U \to Y + A(X, Z, T), W \to 0. \tag{9}$$

2

The linear shear flow is of course the near-wall form of the unperturbed flow and $A(X, Z, T)$ is a displacement function coupled to the pressure by the appropriate pressure displacement law obtained by solving the equations of motion in the main and upper decks.

Main Deck

This layer is relatively passive and transmits the displacement generated in the lower deck to the region above the unperturbed boundary layer. Here u, v, w and p expand as

$$u = U_0(\dot{Y}) + \epsilon C^{1/8}(\frac{T_w^*}{T_\infty^*})^{1/2}(M_\infty^2 - 1)^{-1/8}\lambda^{-3/4}AU_0'(\dot{Y}) + 0(\epsilon^2), \quad (10a)$$

$$v = -\epsilon^2 C^{1/4}\lambda^{1/2}(M_\infty^2 - 1)^{1/4}A_X U_0(\dot{Y}) + 0(\epsilon^2), \quad (10b)$$

$$w = \epsilon^2 C^{1/4}\lambda^{1/2}(M_\infty^2 - 1)^{-1/4}\frac{T_w^*}{T_\infty^*}\frac{R_0(0)Q}{R_0(\dot{Y})}U_0(\dot{Y}) + 0(\epsilon^3), \quad (10c)$$

$$p - p_0 = \epsilon^2 C^{1/4}\lambda^{1/2}(M_\infty^2 - 1)^{-1/4}P(X, Z, t) + 0(\epsilon^3), \quad (10d)$$

together with similar displacement perturbations to the unperturbed temperature and density. Note also that $U_0(\dot{Y})$ and $R_0(\dot{Y})$ are the unperturbed streamwise velocity and density respectively whilst from the spanwise momentum equation the function Q satisfies

$$Q_X = -P_Z. \quad (11)$$

Upper Deck

Here the flow is potential and may be obtained by writing

$$[u, v, w, p] = [1, 0, 0, p_\infty] + \frac{\epsilon^2 C^{1/4}\lambda^{1/2}}{(M_\infty^2 - 1)^{1/4}}[\hat{u}, \hat{v}(M_\infty^2 - 1)^{1/4}, \hat{w}, \hat{p}] + 0(\epsilon^3),$$

and after some simplification we obtain

$$(M_\infty^2 - 1)(\hat{p}_{XX} - \hat{p}_{\overline{Y}\overline{Y}}) - \hat{p}_{ZZ} = 0,$$

$$\hat{p} \to 0, \overline{Y} \to \infty,$$

$$\hat{p} \to P, \frac{\partial \hat{p}}{\partial \overline{Y}} \to \frac{\partial^2 A}{\partial X^2} \text{ as } \overline{Y} \to 0_+. \quad (12)$$

The solution of (12) implies a pressure displacement law which we write symbolically in the form

$$P = \mathcal{L}(A). \quad (13)$$

Thus the nonlinear problem specified by (7), (8), (9), and (13) is now closed and of course must be solved numerically unless some simplification is made. Linear Tollmien-Schlichting waves may be described, following [15], by perturbing about the unperturbed flow $U = Y$. Thus in the lower deck we write for example

$$U = Y + e^{i\{\alpha x + \beta z - \Omega t\}}\tilde{U}(Y)$$

3

and the frequency, and wavenumbers of the disturbance are found to satisfy the eigen relation

$$(i\alpha)^{\frac{1}{3}}(\alpha^2 + \beta^2) = (\frac{A_i'(\xi_0)}{K(\xi_0)})(\frac{\beta^2}{M_\infty^2 - 1} - \alpha^2)^{\frac{1}{2}}, \qquad (14)$$

where $\xi_0 = -i^{-\frac{1}{3}}\Omega\alpha^{-\frac{2}{3}}$, A_i is the Airy function and

$$K = \int_{\xi_0}^\infty A_i(q)dq.$$

The eigenrelation (14) can be solved for a complex wavenumber α for given values of β, M_∞ and Ω. The flow is unstable or stable depending on whether α_i is negative or positive. If we fix β and M_∞ we find that $-\alpha_i$ increases from a negative value when Ω increases from 0. The growth rate then changes sign at Ω_N, the neutral value of Ω, and then increases monotonically until $\Omega = \Omega_M$ where the maximum growth rate is achieved. Beyond $\Omega = \Omega_M$ the growth rate can have further maxima of $-\alpha_i$ but ultimately asymptotes to 0 at large frequencies. Note however that the most unstable wave always corresponds to the first maxima when $\frac{d\alpha_i}{d\Omega} = 0$ and that $-\alpha_i$ remains positive for $\Omega >> 1$. We can alternatively choose to keep α real and find the complex value of Ω.

For weakly nonlinear Tollmien-Schlichting waves it has been shown by Smith [14] and Hall and Smith [7] that nonlinear effects are stabilizing for both two and three dimensional waves. For axisymmetric compressible flows Duck and Hall [3], [4] showed that nonlinear effects are again stabilizing but we know of no results for planar compressible flows. The analysis we shall give is appropriate to strongly nonlinear disturbances but in the small amplitude limit of our theory we will be able to infer the role of nonlinear effects in the weakly nonlinear regime. Strongly nonlinear waves are governed by the full triple deck problem (7)-(8),(1.9), and (13). In general such disturbances must be described by numerical means, here we shall investigate asymptotically large amplitude locally periodic wavesystems.

2 The phase equation for large amplitude waves

The essential ideas of the approach we use can be found in Whitham [21] and were previously used by Hall [6] to discuss the two-dimensional incompressible case. We suppose that a wavesystem moves through the flow and that the local streamwise wavenumber and the frequency of the waves vary slowly as the wavesystem moves downstream. Suppose that the slow temporal and spatial variations of the wave occur over times and lengths of relative size δ^{-1} compared to the period and wavelength of the wave. We introduce slow variable ξ and τ by writing

$$\xi = \delta X, \qquad (15a)$$

$$\tau = \delta t, \qquad (15b)$$

where $0 < \delta << 1$. In order to represent a locally periodic wavesystem we define a phase function θ by writing

$$\theta = \frac{1}{\delta}\Theta(\xi, \tau) + \beta Z. \qquad (16)$$

Here β is a constant spanwise wavenumber and the streamwise wavenumber α and the frequency Ω are then defined by

$$\alpha = \Theta_\xi, \quad \Omega = -\Theta_\tau, \qquad (17)$$

so that α and Ω must satisfy the evolution equation

$$\alpha_\tau + \Omega_\xi = 0. \tag{18}$$

The frequency $\Omega = \Omega(\alpha, \delta)$ may then be found in terms of an asymptotic expansion involving δ and in principle the evolution equation (18) can be solved to determine how α varies in time and space. The definition (2.1)-(2.3) imply that in the triple-deck equations we must use the transformations.

$$\frac{\partial}{\partial X} \to \alpha \frac{\partial}{\partial \theta} + \delta \frac{\partial}{\partial \xi}, \frac{\partial}{\partial t} \to -\Omega \frac{\partial}{\partial \theta} + \delta \frac{\partial}{\partial \tau}, \frac{\partial}{\partial Z} \to \beta \frac{\partial}{\partial \theta}.$$

The lower deck solution for $y = 0(1)$

We expand $U, V,$ and W in the lower deck in the form

$$(U, V, W) = (U_0, V_0, W_0) + \delta^{\frac{1}{3}}(U_1, V_1, W_1) + \ldots \tag{19}$$

where $U_0, V_0,$ etc. are functions of θ, X, Y and τ. In (19) we have anticipated that the appropriate choice of expansion parameter is $\delta^{\frac{1}{3}}$ rather than δ; the reason for this choice will become clear when we investigate the form of the leading order terms in (2.5) in the limit $Y \to \infty$. The pressure is then expanded in the form

$$p = \delta^{-2/3} P_M(\xi, T) + P_0 + \delta^{1/3} P_1 + \ldots \tag{20}$$

where $P_0, P_1,$ etc. are functions of θ, ξ, Y and τ whilst P_M is an induced pressure again implied by the form of (U_0, V_0, W_0) for $Y \gg 1$. The frequency then expands as

$$\Omega = \Omega_0 + \delta^{1/3} \Omega_1 + \ldots,$$

The leading order approximation to (1.7) is then found to be

$$\alpha U_{0\theta} + V_{0Y} + \beta W_{0\theta} = 0$$
$$-\Omega_0 U_{0\theta} + \alpha U_0 U_{0\theta} + V_0 U_{0Y} + \beta W_0 U_{0\theta} = -\alpha P_{0\theta} + U_{0YY},$$
$$-\Omega_0 W_{0\theta} + \alpha U_0 W_{0\theta} + V_0 W_{0Y} + \beta W_0 W_{0\theta} = -\beta P_{0\theta} + W_{0YY},$$
$$P_{0Y} = 0, \tag{21}$$

and we seek a solution of these equations which is periodic in θ. If the displacement function A is expanded as

$$A = A_0 + \delta^{1/3} A_1 + \ldots \tag{22}$$

then the conditions required to close the leading order problem are

$$U_0 = V_0 = W_0 = 0, Y = 0,$$
$$U_0 \to Y + A_0, Y \to \infty,$$
$$P_0 = \mathcal{L}(A_0). \tag{23}$$

The partial differential system (2.7)-(2.9) specifies a nonlinear eigenvalue problem for Ω_0 as a function of α, β and M_∞. We note that the disturbance size can then be changed as a function of α and that solutions will only exist for certain values of α. Moreover it follows that the slow dependence of (U_0, V_0, W_0) and P_0 on ξ, τ arises only through the

5

dependences of these functions on α and Ω_0. In order to solve (2.7)-(2.9) numerically it is convenient to write

$$(U_0, V_0, W_0, P_0) = (U_{00}, 0, W_{00}, P_{00}) + \sum_{\substack{n=-\infty \\ n \neq 0}}^{\infty} (U_{0n}, V_{0n}, W_{0n}, P_{0,n}) e^{in\theta} \tag{24}$$

After a little algebra it is possible to show that the partial differential equation (2.7) can be reduced to

$$V_{0n}'''' - in\{\alpha Y + \alpha U_{00}' + \beta W_{00} - \Omega_0\}V_{0n}'' + iV_{0n}\{\alpha U_{00}' + \beta W_{00}\}'' =$$
$$\sum_{\substack{m \neq n \\ m \neq 0}} \frac{n}{n-m}\{V_{0n-m}''V_{0m} - V_{0n-m}'V_{0m}'\} \tag{25}$$

for $n = \pm 1, \pm 2, \ldots,$

$$\alpha U_{00}'' + \beta W_{00}'' = \sum_{m \neq 0} \frac{i}{m}\{\overline{V}_{0m}V_{0m}' - V_{0m}\overline{V}_{0m}'\}', \tag{26}$$

$$U_{00} = W_{00} = V_{0n} = V_{0n}' = 0, n = \pm 1, \pm 2, \ldots, \quad Y = 0, \tag{27}$$
$$V_{0n}'' = U_{00}' = W_{00}' = 0, \quad Y \to \infty.$$

$$V_{0n}'''(0) = \frac{in\alpha(\alpha^2 + \beta^2)V_{0n}'(\infty)}{\left(\frac{\beta^2}{M_\infty^2 - 1} - \alpha^2\right)^{1/2}}. \tag{28}$$

The last equation is obtained by projecting (1.13) into Fourier space and relating $V_{0n}'(\infty)$, P_{0n} to the corresponding displacement function Fourier component (through continuity) and U_{0n}'', W_{0n}'' at the wall respectively. Of particular importance is the fact that the mean flow correction terms only appear in the leading order nonlinear eigenrelation in the combination $\alpha U_{00}' + \beta W_{00}$ so that we do not need to solve for U_{00} and W_{00} independently. In addition we see that the mean flow functions tend to constants at the edge of the lower deck. We write

$$U_{00} \to A_{00}, W_{00} \to B_{00}, Y \to \infty, \tag{29}$$

and note that A_{00}, B_{00} must in fact depend on the slow variables ξ and τ through the dependence of these quantities on α. This is a crucial result because it means that the mean flow correction has an outer layer structure where $Y\delta\frac{\partial}{\partial\xi} \sim \frac{\partial^2}{\partial Y^2}$. The outer layer is therefore of depth $\delta^{1/3}$ and it is for that reason that our lower deck expansions were previously taken to be in powers of $\delta^{1/3}$ rather than δ. We point out at this stage that the functions $U_{00}, V_{0n}, W_{0n}, P_{0n}, n \neq 0$ do not develop such an outer layer structure because they possess a fast dependence on X through the phase function θ.

Before we discuss the solution in the outer $\delta^{1/3}$ boundary layer it is convenient to write down the order $\delta^{1/3}$ approximation in the $Y = 0(1)$ part of the lower deck. The appropriate differential equations are found to be

6

$$\alpha U_{1\theta} + V_{1Y} + \beta W_{1\theta} = 0, \tag{30a}$$

$$-\Omega_0 U_{1\theta} + \alpha\{U_0 U_{1\theta} + U_1 U_{0\theta}\} + V_0 U_{1Y} + V_1 U_{0Y} +$$
$$\beta\{W_0 U_{1\theta} + W_1 U_{0\theta}\} + \alpha P_{1\theta} - U_{1YY} = \Omega_1 U_{0\theta}, \tag{30b}$$

$$-\Omega_0 W_{1\theta} + \alpha\{U_0 W_{1\theta} + U_1 W_{0\theta}\} + V_1 W_{0Y} + V_0 W_{1Y} +$$
$$\beta\{W_0 W_{1\theta} + W_1 W_{0\theta}\} + \beta P_{1\theta} - W_{1YY} = \Omega_1 W_{0\theta}, \tag{30c}$$

$$P_{1Y} = 0. \tag{30d}$$

The main point to notice here is that $(U_1, V_1, W_1, P_1) = \frac{\partial}{\partial\theta}(U_0, V_0, W_0, P_0)$ is a solution of the homogeneous form of these equations. This is because of the invariance of the 0(1) solution to a Galilean transformation in the X direction. The inhomogeneous form of (2.16) is to be solved subject to

$$U_1 = V_1 = W_1 = 0, \quad Y = 0, \tag{31a}$$

$$P_1 = \mathcal{L}(A_1). \tag{31b}$$

and a condition on $U_1(Y = \infty)$ obtained by a consideration of the outer boundary layer. The condition that the resulting partial differential system should have a solution will determine Ω_1 as a function of α. This enables us to write down the approximation to the phase equation (18) correct upto order $\delta^{1/3}$. In the absence of the outer layer we would write down the conditions $U_1 \to A_1, W_1 \to 0, Y \to \infty$. However the required conditions can only be written down once the solution in the $0(\delta^{1/3})$ diffusion layer has been found.

The diffusion layer

The dominant balance in this layer is between diffusion in the Y direction and convection in the X direction. The thickness of the layer is governed by the balance $U\frac{\partial}{\partial X} \sim \frac{\partial^2}{\partial Y^2}$ and since $U \sim Y$ for $Y \gg 1$, and $\frac{\partial}{\partial X} \sim 0(\delta)$ is follows that the required layer has $Y \sim 0(\delta^{-1/3})$ so we introduce η defined by

$$\eta = \delta^{1/3} Y.$$

We now expand U, V, W and P in the form

$$U = \{\delta^{-1/3}\eta + U_M(\eta) + 0(\delta^{1/3}\} + \left[\hat{U}_0 + \delta^{1/3}\hat{U}_1 + 0(\delta^{2/3})\right], \tag{32a}$$

$$V = \{\delta^{2/3}V_M(\eta) + 0(\delta)\} + \left[\hat{V}_0 + \delta^{1/3}\hat{V}_1 + 0(\delta^{2/3})\right]\delta^{1/3}, \tag{32b}$$

$$W = \{W_M(\eta) + 0(\delta^{1/3})\} + \left[\hat{W}_0 + \delta^{1/3}\hat{W}_1 + 0(\delta^{2/3})\right]\delta^{1/3}, \tag{32c}$$

$$P = \{\delta^{-1/3}P_M + 0(1)+\} + \left[P_0 + \delta^{1/3}P_1 + 0(\delta^{2/3})\right]. \tag{32d}$$

In the above expansions the terms in the curly and square brackets correspond to mean flow correction terms and the wavelike part of the disturbance flow respectively. If we substitute the above expansions into the rescaled form of the lower deck equations and match with the solution in the $Y = 0(1)$ region it is easy to show that

$$\hat{U}_0 = A_0 - A_{00}, \hat{V}_0 = -A_{0\theta}\alpha\eta.$$

7

The mean flow functions U_M, V_M, W_M are determined by the solution of

$$\left.\begin{array}{l} \eta U_{M\xi} + V_M = -P_{M\xi} + U_{M\eta\eta}, \\ U_{M\xi} + V_{M\eta} = 0, \\ U_M = A_{00}, \eta = 0, \\ U_M \to A_M(\xi), \eta \to \infty, \\ P_M = \mathcal{L}(A_M), \end{array}\right\} \tag{33}$$

and

$$\left.\begin{array}{l} \eta W_{M\xi} = W_{M\eta\eta}, \\ W_M = B_{00}, \eta = 0, \\ W_M \to 0, \eta \to \infty. \end{array}\right\} \tag{34}$$

These systems are most easily solved by taking a Fourier transform with respect to ξ and indeed (33) has been solved previously in the context of linearized triple deck theory by Stewartson [17] and Smith [12]. For our purposes here we only need the quantities $U_{M\eta}, W_{M\eta}$ evaluated at $\eta = 0$. We obtain

$$U_M'(0) = J_1(\xi, \tau) = -\frac{3A_i(0)}{2\pi} \int_{-\infty}^{\infty} S(\xi - \phi) A_{00}'(\phi) d\phi,$$

$$W_M'(0) = J_2(\xi, \tau) = \sqrt{\frac{3}{2\pi}} \frac{1}{3^{1/3}} \frac{1}{A_i(0)} \int_{-\infty}^{\xi} \frac{1}{(\xi - \phi)^{1/3}} B_{00}'(\phi) d\phi, \tag{35}$$

where

$$S(\phi) = \int_0^{\infty} \frac{\psi^{4/3}(1 + \psi^{1/3}) e^{-\theta\psi}}{1 + \psi^{4/3} + \psi^{8/3}} d\psi, \phi > 0,$$

$$S(\phi) = \frac{3\pi}{2\sqrt{2\pi}} e^{\theta\phi}, \phi < 0$$

with

$$\theta = -3A_i'(0).$$

The functions $\hat{U}_1, \hat{V}_1$ and $\hat{W}_1$ are then found in terms of U_M and W_M. We obtain

$$\hat{V}_1 = -\alpha A_{0\theta} U_M - \beta A_{0\theta} W_M - \alpha Q_{0\xi}, \tag{36}$$

$$\alpha \hat{U}_1 + \beta \hat{W}_1 = (A_0 - A_{00})(\alpha U_M' + \beta W_M') + Q_0 \alpha. \tag{37}$$

where Q_0 is to be determined by matching with the main deck solutions. When $\eta \to \infty$, $U_M', W_M' \to 0$ so that $Q_0 = A_1$.

It remains for us to match (2.22), (2.23) with the solution in the $Y = 0(1)$ part of the lower deck. In the first instance we note that $U_M \sim J_1\eta, W_M \sim J_2\eta$ for small η so it is convenient to write

$$U_1 = \hat{U}_1 + J_1\eta, W_1 = \hat{W}_1 + J_2\eta,$$

in (2.16) to give

$$\alpha \hat{U}_{1\theta} + \hat{V}_{1Y} + \beta \hat{W}_{1\theta} = 0,$$

$$-\Omega_0 \hat{U}_{1\theta} + \alpha(U_0 \hat{U}_{1\theta} + \hat{U}_1 U_{0\theta}) + V_0 \hat{U}_{1Y} + \hat{V}_1 U_{0Y} + \beta(W_0 \hat{U}_{1\theta} + \hat{W}_1 U_{0\theta})$$

$$+\alpha P_{1\theta} - \hat{U}_{1YY} = \Omega_1 U_{0\theta} - \alpha J_1\eta U_{0\theta} - V_0 J_1 - \beta J_2\eta U_{0\theta}$$

$$-\Omega_0 \hat{W}_{1\theta} + \alpha(U_0 \hat{W}_{1\theta} + \hat{U}_1 W_{0\theta}) + \hat{V}_1 U_{0Y} + V_0 W_{1Y}$$

$$+ \beta\{W_0 \dot{W}_{1\theta} + \dot{W}_1 W_{0\theta}\} + \beta P_{1\theta} - W_{1YY} \tag{38}$$

$$= \Omega_1 W_{0\theta} - \alpha \eta J_1 W_{0\theta} - V_0 J_2 - \beta J_2 \eta W_{0\theta}.$$

The conditions required to completely specify the problem for $(\dot{U}_1, V_1, \dot{W}_1, P_1)$ are then found to be

$$\dot{U}_1 = \dot{W}_1 = V_1 = 0, V = 0,$$

$$P_1 = \mathcal{L}(A_1),$$

$$- \alpha A_1 + \alpha \dot{U}_1 + \beta \dot{W}_1 \rightarrow (A_0 - A_{00})(\alpha J_1 + \beta J_2), Y \rightarrow \infty. \tag{39}$$

Suppose that we set all the right hand sides in (2.24) equal to zero and replace the above condition by $\alpha \dot{U}_1 + \beta \dot{W}_1 \rightarrow \alpha A_1, Y \rightarrow \infty$. The simplified homogeneous system obtained by this procedure has the solution

$$(\dot{U}_1, V_1, \dot{W}_1, P_1) = (U_0, V_0, \dot{W}_0, P_0)_\theta$$

so that (38), (39) only has a solution if the appropriate solvability condition is satisfied. The condition is most easily obtained by expressing (38) as a system of equations in the form

$$\frac{\partial}{\partial Y}(\chi, V_1, \chi_Y, P_1)^T = B(\chi, V_1, \chi_Y, P_1)^T + C(\chi, V_1, \chi_Y, P_1)_\theta^T + G,$$

where, $\chi = \alpha \dot{U}_1 + \beta \dot{W}_1$, B, C are 4×4 matrices and G is a column vector with elements proportional to $\alpha J_1 + \beta J_2$. The partial differential system adjoint to the homogeneous form of the above system is obtained by multiplying by a vector and integrating over $0 < Y < \infty, 0 < \theta < \frac{2\pi}{\alpha}$. Full details are given in [6] and after some analysis we obtain

$$\Omega_1 = K(\alpha)(\alpha J_1 + \beta J_2) \tag{40}$$

where $K(\alpha)$ may be expressed in terms of integrals involving the adjoint and the $0(1)$ lower deck solution.

Having determined Ω_1 we can now write down the partial differential equation to determine α correct to $0(\delta^{1/3})$. We write

$$\frac{\partial \alpha}{\partial \tau} + \Omega_0'(\alpha)\frac{\partial \alpha}{\partial \xi} + \delta^{1/3} \{K(\alpha)(\alpha J_1 + \beta J_2)\}_\xi = 0. \tag{24}$$

If α is then specified at $\tau = 0$ we can integrate (24) forward in time to determine the evolution of α.

3   The modulational instability of uniform wavetrains

It can be seen from (24) that a particular solution of the wavenumber evolution equation is

$$\alpha = \alpha_0$$

where α_0 is a constant so that the wavenumber and frequency of the wave remain constant as it propagates downstream. In order to investigate the modulational instability of the uniform wavetrain we write

$$\alpha = \alpha_0 + \Delta$$

9

with $|\frac{\Delta}{\alpha_0}| << 1$. It follows from (24) that Δ satisfies

$$\frac{\partial \Delta}{\partial \tau} + \left[\Omega_0'(\alpha_0) + \Delta\Omega_0''(\alpha_0) + 0(\Delta^2)\right]\frac{\partial \Delta}{\partial \xi} + \delta^{1/3}K(\alpha_0)\frac{\partial}{\partial \xi}\left[\alpha_0\hat{J}_1 + \beta\hat{J}_2\right] = 0(\delta^{1/3}\Delta^2).$$

Here J_1 and J_2 are defined by

$$\hat{J}_1 = -\frac{3A(i(0)}{2\pi}A_{00}'(\alpha_0)\int_{-\infty}^{\infty}S(\xi - \phi)\frac{\partial \Delta}{\partial \phi}d\phi,$$

$$\hat{J}_2 = \sqrt{\frac{3}{2\pi}}\frac{1}{3^{1/3}}\frac{B_{00}'(\alpha_0)}{A_i(0)}\int_{-\infty}^{\xi}\frac{\partial \Delta}{\partial \phi}\frac{1}{(\xi - \phi)^{1/3}}d\phi.$$

By a suitable transformation we can eliminate the term in the wavenumber evolution equation proportional to $\Omega_0'(\alpha_0)$. If we then introduce a scaled time variable $Y \sim \delta^{1/3}\tau$, and amplitude $\Delta \sim 0(\delta^{-1/3})\Delta$ then we see that the canonical form for the evolution equation is

$$\frac{\partial \Lambda}{\partial T} + \Lambda\frac{\partial \Lambda}{\partial \xi} = \pm\frac{\partial}{\partial \xi}\int_{-\infty}^{\infty}\frac{\partial \Lambda}{\partial \phi}\left\{\frac{H(\xi - \phi)}{(\xi - \phi)^{1/3}} + \gamma S(\xi - \phi)\right\}d\phi \qquad (25)$$

Here H is the Heaviside function and γ is defined by

$$\frac{1}{\gamma} = -\frac{\beta_0 B_{00}'(\alpha_0)}{\alpha_0 A_{00}'(\alpha_0)}\frac{\sqrt{2\pi}}{3^{1/6}}\frac{1}{A_i^2(0)}. \qquad (26)$$

Calculations show that $\frac{B_{00}'}{A_{00}'}$ is always negative so that γ is a positive constant. Finally the $\pm$ sign in (25) are to be taken depending on whether $B_{00}'(\alpha_0)K(\alpha_0)$ is positive or negative. Computations which we shall report on in the next section show that both possibilities occur.

In the absence of the viscous like terms on the right hand side of (25) we see that Λ satisfies the inviscid Burgers equation which for rather arbitrary initial data will develop shocklike solutions. The viscous terms will then become important in such rapidly varying regions. The kernel function S appearing in (25) can then be simplified using its asymptotic form for small argument. Thus using the result

$$S(\phi) \sim \frac{1}{\theta 1/3}T(1/3)\phi^{-1/3}+, 0 < \phi << 1,$$

$$S \sim \frac{3\pi}{2\sqrt{2\pi}}, \phi < 0,$$

we deduce that a rescaled form of (25) is

$$\frac{\partial \Lambda}{\partial T} + \Lambda\frac{\partial \Lambda}{\partial \xi} = \pm\frac{\partial}{\partial \xi}\int_{-\infty}^{\xi}\frac{\partial \Lambda}{\partial \phi}\frac{1}{(\xi - \phi)^{1/3}}d\theta \qquad (27)$$

and we shall now concentrate our attention on this equation.

4 Numerical solution of the 0(1) problem

Here we discuss the results we have obtained for the solution of the nonlinear eigenvalue problem $\Omega_0 \equiv \Omega_0(\alpha, \beta, M_\infty)$ associated with the 3D periodic triple deck problem (2.7)-(2.9). The calculations were carried out using a finite difference method in the Y direction and a Fourier spectral method in the θ direction. The nonlinear terms were accounted for by an iterative process with only the linear terms evaluated at the new level of iteration. We restricted our attention to three Mach numbers, $M_\infty = 1.1, 1.25, 1.5$. Figure 1 shows the dependence of α on β for the linear neutral modes at these Mach numbers. The corresponding frequencies are shown in Figure 2.

Figures 3-5 show a variety of $\Omega_0 - \alpha$ plots for three different values of M_∞ and a selection of spanwise wavenumbers. The circle shown in the figures corresponds to the linear neutral point in $\Omega_0 - \alpha_0$ space. Thus one end of each of the curves connects the zero amplitude state with an initially small amplitude wave whilst the other end of each curve represents the points at which our iteration procedure failed to converge. In each case we used 32 modes in the periodic variable θ, 400 in the normal direction and infinity was taken to be 15. At the point on each curve where the iteration procedure failed to converge we calculated the wall shear stress but there was no sign of it changing sign. We have no explanation why our iteration procedure could not be continued further and it is possible that, as was found in [6] for the incompressible case, the Fourier expansion procedure fails to converge at this stage and the disturbance develops a singularity.

Figures 3a-i show results at a Mach number 1.1. At moderate wavenumbers, Figures 3c-g, we see that there is a supercritical bifurcation to a finite amplitude state at the linear neutral point. This is similar to the situation discussed for subsonic flow by Hall (1995). However in Figures 3b,h we see that in the weakly nonlinear limit the wavenumber initially decreases as the amplitude increases. Since the frequency initially increases in this regime the bifurcation remains a supercritical one with the bifurcating solution temporally stable. However for sufficiently small or large wavenumbers, Figures 3a,i, we find that both the frequency and wavenumber decrease with increasing disturbance amplitude in the weakly nonlinear limit. Thus the bifurcation is now subcritical and nonlinear effects are destabilizing.

Thus all disturbances apart from those with sufficiently small or large spanwise wavenumber bifurcate supercritically. The modes with moderate spanwise wavenumber bifurcate subcritically.

In Figures 4a-f we show results for a Mach number 1.25. The results are similar to those described previously for $M_\infty = 1.1$. However we see that the supercritical behaviour is now restricted to a smaller band of spanwise wavenumbers. If the Mach number is further increased we ultimately reach a stage where the bifurcation is always subcritical; see Figures 5a-e.

Finally it remains here for us to discuss the sign of the constant $B'_{00}(\alpha_0)K(\alpha_0)$ which in effect determines whether the viscous-like derivative appearing on the right hand side of (3.1) is stabilizing or destabilizing. We recall that in in the subsonic case it was found in [6] that viscous effects were always found to be destabilizing so that the negative sign in (3.1) was to be taken. In the present problem we found a similar result for every case when the initial bifurcation has both frequency and wavenumber increasing with the disturbance amplitude. In every other case we computed we found that viscous effects were stabilizing if the equilibrium value of α initially decreased with disturbance

11

amplitude. Thus it is necessary for us to discuss the solutions of (3.1), or in fact more appropriately (3.3), for both cases.

5 Numerical solution of the phase equations

In this Section we are concerned with the numerical solution of the canonical phase equation (3.3). The integral term on the right hand side is a fractional derivative of order $\frac{4}{3}$ and is most easily dealt with in Fourier space. A fractional derivative of order p is defined by

$$\frac{\partial^p \Lambda}{\partial \xi^p} \equiv \frac{1}{\Gamma(1-p)} \int_{-\infty}^{\xi} \frac{\frac{\partial \Lambda}{\partial \phi}}{(\xi - \phi)^p} d\phi.$$

For a discussion of fractional calculus the reader is referred to [10]. The Fourier transform gives

$$\mathcal{F}\left(\frac{\partial^p \Lambda}{\partial \xi^p}\right) = (ik)^p \mathcal{F}(\Lambda),$$

where $\mathcal{F}(u) = \int_{-\infty}^{\infty} u e^{-ik\xi} d\xi$. According to a rescaling of Λ similar to that of Section 3, the canonical equation (3.3) is cast into the form

$$u_t + u u_x = \pm \nu \frac{\partial^{4/3} u}{\partial x^{4/3}},$$

$$(x, t) \in \mathbf{R}^1 \times \mathbf{R}^+, \tag{28}$$

$$u(x, 0) = u_0(x), u(x + 2\pi, t) = u(x, t).$$

Here $\nu > 0$ and can be re-scaled to unity by changing the initial condition, for instance. The boundary conditions in (5.1) indicate that we are considering the spatially periodic problem since our main interest lies in the prediction of local structures such as finite-time infinite slope singularities, for example. Equations containing fractional derivatives have been derived and studied by other authors in the context of boundary layer stability, [1], and nonlinear acoustic waves, [19]. The former work derives an equation with negative diffusion and a $\frac{1}{2}$ spatial derivative, while the latter study considers a positive diffusion and a fractional derivative of $\frac{1}{3}$ together with the usual stabilizing Burgers diffusion (second spatial derivative and positive diffusion). The former authors conjecture and formally analyze the formation of a "shock" singularity driven by the inviscid Burgers equation, to leading order. Our numerical results for the present problem lend support to such breakups. The analysis and numerical experiments in [19] do not produce shocks due to the presence of the stabilizing second derivative term; this is brought into the evolution as a higher order correction once a shock begins to form. In the present problem a hierarchy of higher derivatives enter simultaneously and consequently the evolution in the "inner" region is governed by the full unsteady triple deck problem which is hard to analyze in order to obtain jump conditions, for instance.

A linearization of (5.1) leads to normal mode solutions

$$u = A e^{\pm \nu (ik)^{4/3} t} + c.c = A e^{\pm \nu (1/2)(-1 + i\sqrt{3}) k^{4/3} t} + c.c., \tag{29}$$

where $c.c.$ denotes complex conjugate. We see from (5.2), therefore, that the system is linearly stable or unstable respectively, depending on the sign chosen. The linearly stable

12

case provides a nonlinear evolution problem which can be compared with the viscous Burgers equation. There are two essential differences, however: First the amount of diffusion is less (for large k it is of order $k^{4/3}$ as opposed to k^2 for the Burgers equation), and second, the linear solution contains a dispersive part in contrast to the purely diffusive nature of the linearized viscous Burgers equation. The latter fact requires some care in the numerical treatment described later. The main question we address numerically is whether the dissipation in the present problem is sufficient to prevent infinite slope singularities - the numerical evidence suggests that shocks do tend to form. The situation with the negative sign in (5.1) is worse in that the problem is now ill-posed and solutions may exist for small enough times if the initial conditions are chosen appropriately. This class of numerical experiment also suggests the generic formation of infinite slope singularities or "shocks".

The numerical scheme used is a pseudospectral one which allows a straightforward representation of the fractional derivative. All derivatives are computed by a forward Fast Fourier Transform (FFT) along with the appropriate inverse FFT, and the time-marching is done in real space by an adaptive second or third order accurate scheme. In order to monitor the accuracy of the solution as the computation evolves, we utilized the conserved quantity

$$\frac{\partial}{\partial t}\left(\int_0^{2\pi} u(x,t)dx\right) = 0. \tag{30}$$

Most numerical experiments have initial condition $u_0(x) = \sin(x)$ and so $\int_0^{2\pi} u(x,t)dx = 0$ throughout the evolution. All results reported here satisfy (5.3) to within computer round-off errors. Before presenting numerical results we mention some accuracy requirements of the numerical schemes. In view of the linear solution (5.2), it is seen that when the kth Fourier component is stepped forward in time by an amount Δt (according to a time-split scheme for instance - this is a useful simplification to get an estimate of the accuracy requirements) the solution due to the linear operator is given by

$$\hat{u}_k(t + \Delta t) = e^{\pm \nu(1/2)(-1+i\sqrt{3})k^{4/3}\Delta t}\hat{u}_k(t). \tag{31}$$

If a computation is performed with n modes, then the maximum available Fourier component is $k_{max} = \frac{n}{2}$ (in practice k_{max} is smaller than $n/2$ due to filtering); the complex part in the exponential in (5.3) causes a rotation which will be spurious unless $\beta = \frac{1}{2}\sqrt{3}\nu k_{max}^{4/3}\Delta t$ is small enough. This places a restriction on the value of Δt. All runs reported here have $\beta < 0.1$, and it is seen that the step size needs to be decreased as the resolution increases.

The first set of results presented below have $\nu = 0.1$ and an initial condition $u_0(x) = \sin(x)$. All numerical experiments terminate in infinite slope singularities after a finite time and so a "shock" is seen to form then. The maximum absolute value of the slope that can be computed accurately depends on the spatial resolution and it was found that an amplification in $max(|u_x|)$ of over 80 is possible to achieve accurately with 4096 modes. Numerical convergence has also been established by a comparison between this run and a lower resolution run. Unless otherwise stated the results shown in the following figures have been computed with $n = 4096$.

Figure 6(a) shows the evolution of $u(x,t)$ and Figure 6(b) depicts the final computed profile. The maximum value of the magnitude of the slope is 80.03 by the end of the computation, and it occurs at $t = 1.246$. It is seen that the solution steepens up as the computation evolves and due to the dispersive part of the pseudo-differential operator

13

the position of maximum $|u_x|$ is not constant but varies slightly. Next we consider the evolution of the maximum magnitude of u_x in Figure 7 which again indicates that the slope is blowing up after a finite time. We note that the initial value of this quantity is 1 and by the end of the computation a magnification factor of 100 has taken place. The energy of the solution defined as $\int_0^{2\pi} u^2(x,t)dx$ remains bounded as t increases and in fact decreases monotonically; this is shown in Figure 8.

Further quantitative information about the suggested singularity can be obtained by considering the evolution in time of the spectral amplitude of the solution. Given a time t, say, the discrete Fourier transform of u is computed and is denoted by $\hat{u}_k$ for $k = -\frac{n}{2}, \ldots, \frac{n}{2}$; it is sufficient to consider those spectral components with positive k (note that the component corresponding to $k = 0$ is zero due to the conservation of the integral of u) since $u(x,t)$ is a real function and so the sequence $\{\hat{u}_k\}$ is Hermitian, i.e. $\hat{u}_{-k} = \hat{u}_k^*$ where $*$ denotes complex conjugate. We define a spectral amplitude, therefore, at a given time t by

$$S(k,t) = |\hat{u}_k(t)|, \qquad k = 1, \ldots, \frac{n}{2} - 1.$$

In Figures 9 and 10 we depict $S(k,t)$ versus k and $\ln(S(k,t))$ versus $\ln(k)$ at different times. The times correspond exactly to the times at which the profiles in Figure 5 are shown and are therefore the spectral amplitude characteristics of those profiles. In both Figures 9 and 10 as time increases the spectral amplitude increases upwards. In order to capture the behavior of the spectrum for large k we follow [20] and assume that the spectrum has the following behavior for large k,

$$\hat{u}_k(t) = c(t)k^{-\alpha(t)}e^{-\delta(t)k}. \tag{32}$$

The form (5.5) is suggested by the large k behavior of the Fourier transform of an analytic function with isolated singularities in the complex plane. The dominant behavior contained in (5.5) comes from the singularity in the upper half-plane nearest to the real axis which is not a multiple pole (for details see [20] and [2]). We used the results of Figures 9 and 10 to estimate the parameters in (5.5) as the computation evolved towards a singularity. We note that $\delta(t)$ decreases to zero as the singularity is approached and the computation is inaccurate once the value of δ becomes smaller than the mesh size (this accuracy requirement is observed by all the results given here). We used least squares fits to estimate $\alpha(t)$ and $\delta(t)$. It follows from (5.5) that

$$\ln |\hat{u}_k| = -\alpha(t)\ln(k) - k\delta(t) + D(t), \tag{33}$$

where, for notational convenience, α and δ in (5.6) are real numbers which correspond to their respective real parts in (5.5). It follows from (5.6) that log-linear and log-log plots will provide estimates for $\delta(t)$ and $\alpha(t)$ respectively. The former evolution can be found in Figure 9 and the latter in Figure 10. The results for our estimates are given in Figure 11 and summarized in Tables 1 and 2 which contain additional information on the modes retained for the fit. The spacing between grid points for 4096 modes is 0.0015 and is larger than the minimum value of δ reached by the end of the computation. The numerical results can be used to conjecture the terminal form of the solution. It appears that the dominant structure is that provided by the inviscid Burgers breakdown - the inviscid Burgers has a power law dependence of $\alpha = 4/3$ due to the local $x^{1/3}$ behavior in the neighborhood of the singularity. At times above $t = 1.24$ a power law of 1.33 is achieved suggesting that it is the inviscid Burgers mechanism which is controlling the local structure of the singularity.

14

t	α	Modes retained for fit
0.7	3.03	$2 \leq k \leq 8$
.8	2.61	$2 \leq k \leq 10$
.9	2.38	$2 \leq k \leq 20$
1.0	2.06	$5 \leq k \leq 30$
1.1	1.76	$10 \leq k \leq 60$
1.2	1.42	$10 \leq k \leq 100$
1.21	1.39	$10 \leq k \leq 100$
1.22	1.37	$10 \leq k \leq 100$
1.23	1.35	$10 \leq k \leq 100$
1.24	1.33	$10 \leq k \leq 100$
1.246	1.33	$10 \leq k \leq 100$

Table 1

t	δ	Modes retained for fit
0.7	0.377	$30 \leq k \leq 70$
.8	0.168	$40 \leq k \leq 150$
.9	0.099	$50 \leq k \leq 250$
1.0	0.051	$50 \leq k \leq 490$
1.1	0.021	$500 \leq k \leq 1150$
1.2	0.0082	$1000 \leq k \leq 2000$
1.21	0.0076	$1000 \leq k \leq 2000$
1.22	0.0071	$800 \leq k \leq 1800$
1.23	0.0067	$800 \leq k \leq 1800$
1.24	0.0063	$800 \leq k \leq 1800$
1.246	0.0060	$800 \leq k \leq 1800$

Table 2

Another quantity which provides positive evidence of an inviscid Burgers breakdown is given by the enstrophy of the solution defined by

$$2\mathcal{E}(t) = \int_0^{2\pi} u_x^2 dx. \tag{34}$$

The evolution of $\mathcal{E}(t)$ corresponding to the runs described above is given in Figure 12. In order to make a comparison with the inviscid Burgers analogue, it is useful to give the solution then, corresponding to $\nu = 0$. Using characteristic coordinates an implicit form of the solution is (see [9])

$$u(t, x(t, s)) = u_0(s),$$

$$x(t, s) = s + tu_0(s).$$

The slope u_x follows from these results and is

$$u_x = \frac{u_0'(s)}{1 + tu_0'(s)},$$

15

showing that an infinite slope singularity is encountered after a finite time given by

$$T = \frac{1}{-Inf[u_0'(s)]}.$$

An estimate of the rate at which $\mathcal{E}(t)$ blows up as the singular time is approached is best achieved by using Lagrangian coordinates; this is described in [5] and we simply sketch the result. In Lagrangian coordinates the enstrophy is

$$2\mathcal{E}(t) = \int_0^{2\pi} \frac{(u_0'(s))^2}{1 + tu_0'(s)} da.$$

If the singular time is t_*, then it follows from a local expansion of u_0 near $s = 0$ (without loss of generality the singularity is taken to occur here) that

$$u_0'(s) = -\frac{1}{t_*} + \frac{1}{2}u_0'''(0)s^2 + O(s^3),$$

which on insertion into (5.7) and retainment of the leading order term as $t \to t_* -$, gives

$$\mathcal{E}(t) \sim (t_* - t)^{-\frac{1}{2}}, \qquad t \to t_* - . \tag{35}$$

The local $x^{1/3}$ structure of u near the singular time also follows from the Lagrangian formulation (see [5] for more details). The results given above are valid for the inviscid Burgers equation and in general the singular time t_* is different from that of (5.1) denoted by t_s.

In what follows, then, we show that our numerical results with $\nu \neq 0$ are consistent with the asymptotic blowup rate (5.8). Referring to Figure 12 we see that $\mathcal{E}$ is becoming singular after a finite time; the value of t_s is not provided directly by the computations, and in order to check the algebraic rate (5.8) it is necessary know the value of t_s. In the absence of a rigorous way of obtaining t_s we proceed as follows: reasonable guesses are made for t_s, consistent with the data in Figure 12, and plots of $\ln(\mathcal{E}(t))$ versus $\ln(t_s - t)$ are generated (for brevity we do not include those plots here). If a power law behavior is present for small values of $(t_s - t)$, then the plots above are linear with the slope giving an estimate of the power. Least squares fits were applied for a range $1.226 \leq t \leq 1.246$ (a typical corresponding range in the log-log plots is $[-2.9, -2.59]$) to gain an estimate of the power law for comparison with (5.8) which has a power law behavior of $-\frac{1}{2}$. The results are given in Table 3 below. The numerical values are consistent with those predicted by the local analysis providing additional evidence that it is the singularity formation of the inviscid Burgers equation which is dictating the singularity structure.

t_s	1.29	1.3	1.301	1.3025	1.305	1.31
slope	-0.41	-0.49	-0.50	-0.51	-0.53	-0.57

Table 3

5.1 Negative diffusion case

In this section we consider the evolution when the "diffusion" is negative and the minus sign is in effect in equation (5.1). In view of the linearized solution (5.4) the problem

16

now contains a short wave instability with growth of the order $\exp(k^{4/3}t)$; we note that this is worse than the well-known Kelvin-Helmholtz instability whose nonlinear evolution has been treated numerically by [8], for example. Due to the short wave instability, numerical round-off errors are viewed by the system as low amplitude high wavenumber perturbations; the shorter the wavelength the faster the initial (exponential) growth will be and unless such perturbations are removed their eventual growth and nonlinear interactions contaminate the flow and produce a spurious numerical solution. This problem is overcome numerically by filtering out (setting to zero) any Fourier coefficient below a certain tolerance level; we use the same filter for all wavenumbers in much the same way as was done in [8] for Kelvin-Helmholtz instability and in [11] for a system with a worse dispersion relation than Kelvin-Helmholtz flow. This filtering technique was also applied to the positive diffusion case described earlier.

The presence of the short-wave instability, then, means that nonlinear solutions will exist for small enough times if the initial conditions are chosen appropriately. To illustrate this consider the evolution equation with the bad sign

$$u_t + uu_x = -\nu\frac{\partial^{4/3}u}{\partial x^{4/3}}, \qquad \nu > 0. \tag{36}$$

Given an initial condition at $t = t_0$, say, a backwards integration in time is well-posed, to times prior to any singularity encounter at least (care is required since the positive diffusion case can encounter an infinite slope singularity if the solution is evolved long enough), since the diffusive effect appears positive then. Initial conditions which satisfy (5.9) can thus be generated. Typically we integrated (5.9) from an initial condition $u_0(x)$ at t_0, to $t = 0$ and there switched to a forward time integration. In the numerical results described below, we have $t_0 = 0.05$ and $u_0 = \sin(x)$. The number of modes used is 4096 and the filter level is set at 10^{-12}.

The evolution from $t = 0$ to $t = 0.91$ is given in Figure 13. Profiles are plotted every 0.05 time units and the profile at $t = 0.91$ is included also. Again we see that the solution is steepening and an infinite slope singularity appears after a finite time; the minimum slope at $t = 0.91$ is approximately -20. In addition, the maximum (or minimum) of the solution increases with time as opposed to the behavior for positive ν described previously. In fact the energy of the solution increases monotonically now, as expected. These features of the evolution are given in Figure 14 which depicts the evolution with time of the maximum of $|u_x|$, the enstrophy (defined earlier) and the energy. These results strongly suggest that the numerical solution is encountering an infinite slope singularity after a finite time. We have also checked the power law (5.8) for the enstrophy with favorable results; it is found that a singular time between 0.93 and 0.94 gives the power law (5.8) for our numerical data of Figure 13. We also note that the numerical solution becomes unstable soon after $t = 0.91$; in particular we were not able to achieve, with desirable accuracy, the minimum slopes of -80 or less which were achieved for positive diffusion.

Finally we consider the evolution of the spectra of the solution. As before, we present log-linear and log-log plots analogous to those of Figures 9 and 10. Results are plotted at time intervals of 0.05 for $0 \leq t \leq 0.65$ and at intervals of 0.005 for $0.65 < t \leq 0.91$. The reason for this refinement is due to the rapid change of the spectrum as the singularity is approached. The log-linear plots are given in Figure 15 and the corresponding log-log ones in Figure 16.

As can be seen from Figures 15 and 16 there are some different features in the spectrum from that corresponding to positive diffusion. In particular an oscillatory behavior appears at large wavenumbers and a kink in the spectrum is clearly seen at a time just below 0.91. Such features were absent in the positive diffusion case and can be explained by the influence of higher singularities moving down in the complex plane towards the real axis; the interaction of several such singularities can produce oscillatory behavior in the spectrum at large k. For an explicit example of this the reader is referred to the text [2] (p. 256). We also tried to estimate the power law behavior of the spectrum in order to compare with the positive diffusion results. Such an estimate can be derived from the data of Figure 16 by the same techniques described previously. It has been found that for the times up to which the integration has been carried out, the best estimate of the slope coming from intermediate values of $\ln(k)$ in Figure 16, is approximately -1.78; this is approximately 25% different from the estimate found earlier and for the inviscid Burgers behavior. The solution suffers from short wave instabilities immediately after $t = 0.91$ (these can be seen creeping in at the largest values of k already) and it is possible that a k-dependent filter can increase the time of integration and allow further convergence in the power law estimate. We emphasize, however, that the estimate -1.78 is a consistent transient with the inviscid Burgers singularity and further careful numerical experiments are required to verify this.

6   Conclusion

We have investigated in detail the solution of the modulation equation for large amplitude waves in a compressible boundary layer. The equation in question, (3.3), was solved for the cases of both negative and positive diffusion. The evolution equation describes the evolution of a wavenumber perturbation to a uniform wavetrain. In both cases we found that with periodic initial data the solution breaks down and a singularity forms. After the onset of the singularity the full triple deck problem must be solved. However our results show that large amplitude waves in supersonic flows cannot persist with constant wavenumber and frequency.

References

[1] Brotherton-Ratcliffe, R.V. and Smith, F.T. 1987 Complete breakdown of an un-steady interactive boundary layer (over a surface distortion or in a liquid layer), *Mathematika* **34**, 86-100.

[2] Carrier, G.F., Krook, M. and Pearson, C.E. *Functions of a complex variable, theory and technique*, Hod Books, Ithaca, New York, 1983.

[3] Duck, P.W. and Hall, P., 1989, On the interaction of Tollmien-Schlichting waves in axisymmetric supersonic flows. *QJMAM*, **42**, 115-130.

[4] Duck, P.W. and Hall, P., 1990, Non-axisymmetric viscous lower branch modes in axisymmetric supersonic flow. *J. Fluid Mech.*, **213**, 191-201.

[5] Fournier, J.-D. and Frisch, U. 1983 L'équation de Burgers déterministe et statistique, *Journal de Méchanique Théorique et Apliquée* **2**, No. 5, 699-750.

[6] Hall, P. 1994 A phase equation approach to boundary layer transition:Toll mien-Schlichting waves. To appear in Journal of Fluid Mechanics.

[7] Hall, P. and Smith, F.T. 1984, On the effects on Nonparallelism, Three Dimension-ality and MOde Interaction in Nonlinear boundary layer stability, Studies in Applied Maths., **70**, 91,121.

[8] Krasny, R. 1986 A study of singularity formation in a vortex sheet by the point vortex approximation, J. Fluid Mech. **167**, 65-93.

[9] Lax, P.D. Hyperbolic Systems of Conservation Laws and the Mathematical Theory of Shock Waves, SIAM Regional Conference Series in Applied Mathematics, No. 11, 1972.

[10] Oldham, K.B. and Spanier, J. *The Fractional Calculus*, Academic Press, 1974.

[11] Papageorgiou, D.T. and Smith, F.T. 1988 Nonlinear stability of the wake behind a flat plate placed parallel to a uniform stream, *Proc. R. Soc. Lond. A* **419**, 1-28.

[12] Smith, F.T. 1973 Laminar flow over a small hump. *J. Fluid Mech.*, **57**, 803,824.

[13] Smith, F.T. 1979a On the non-parallel flow stability of the Blasius boundary layer. *Proc. R. Soc. Lond.* **A366**, 91.

[14] Smith, F.T. 1979b Nonlinear stability of boundary layers for disturbances of various sizes. *Proc. R. Soc. Lond.* **A368**, 573 (also corrections 1980, **A371**, 439-440).

[15] Smith, F.T. 1989 On the first-mode instability in subsonic, supersonic or hypersonic boundary-layers. *J.Fluid Mech* **198**, 127-154.

[16] Stewartson, K., 1964. *Theory of laminar boundary layers in compressible fluids.* Oxford University Press.

[17] Stewartson, K. 1969. On the flow near the trailing edge of a flat plate. *Mathematika*, **16**, 106,121.

[18] Stewartson, K. and Williams, P. G. 1969. Self-induced separation. *Proc. R. Soc. Lond.*, **A312**, 181-206.

[19] Sugimoto, N. 1991 Burgers equation with a fractional derivative; hereditary effects on nonlinear acoustic waves, *J. Fluid Mech.* **225**, 631-653.

[20] Sulem, C., Sulem, P.-L. and Frisch, H. 1983 Tracing complex singularities with spectral methods, *J. Comput. Phys.* **50**, 138-161.

[21] Whitham, G.B. 1977 *Linear and Nonlinear Waves*. Wiley.
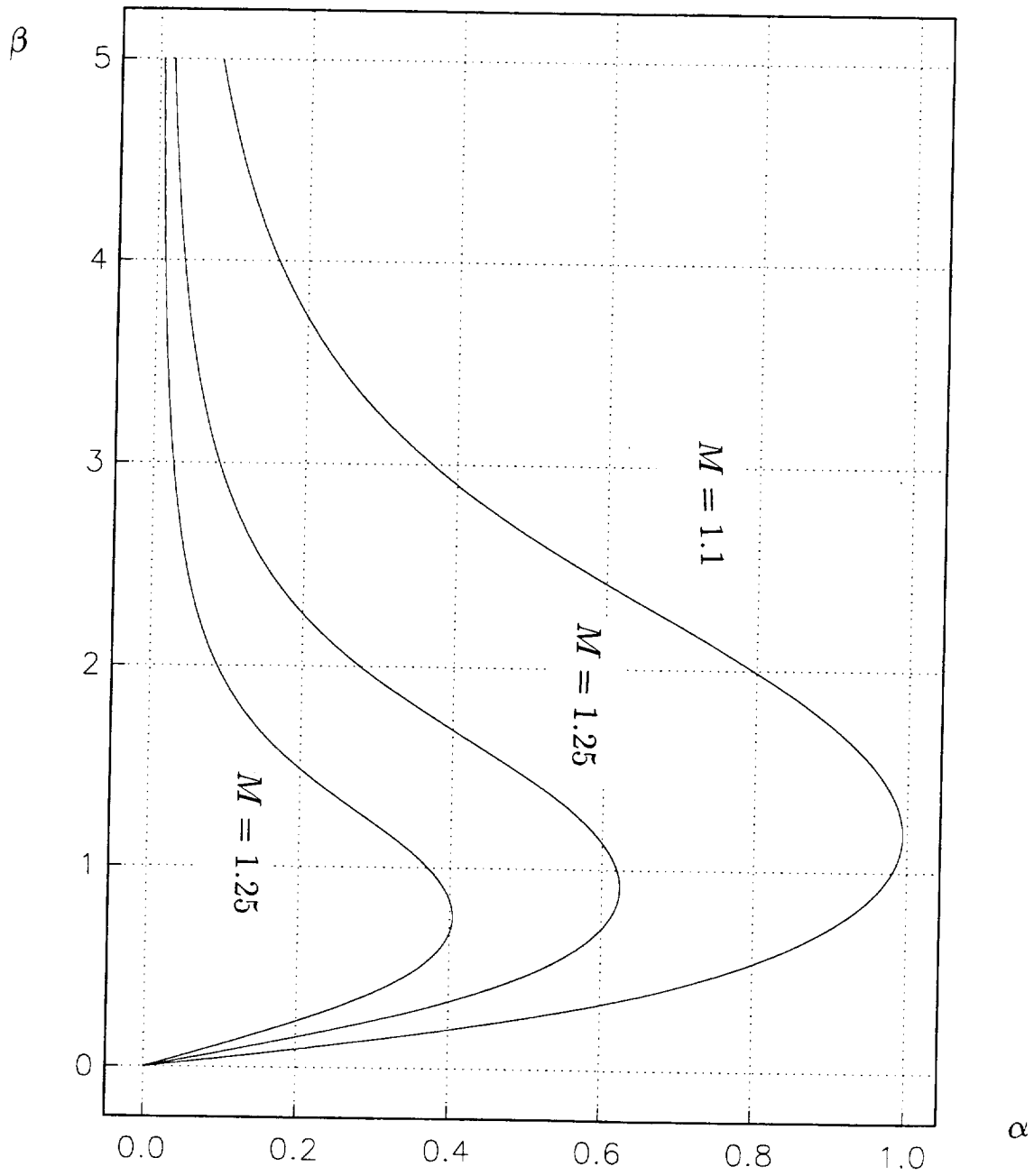
- **Figure 1** The dependence of the neutral linear wavenumber α on the spanwise wavenumber β for $M_\infty = 1.1, 1.25, 1.5$.
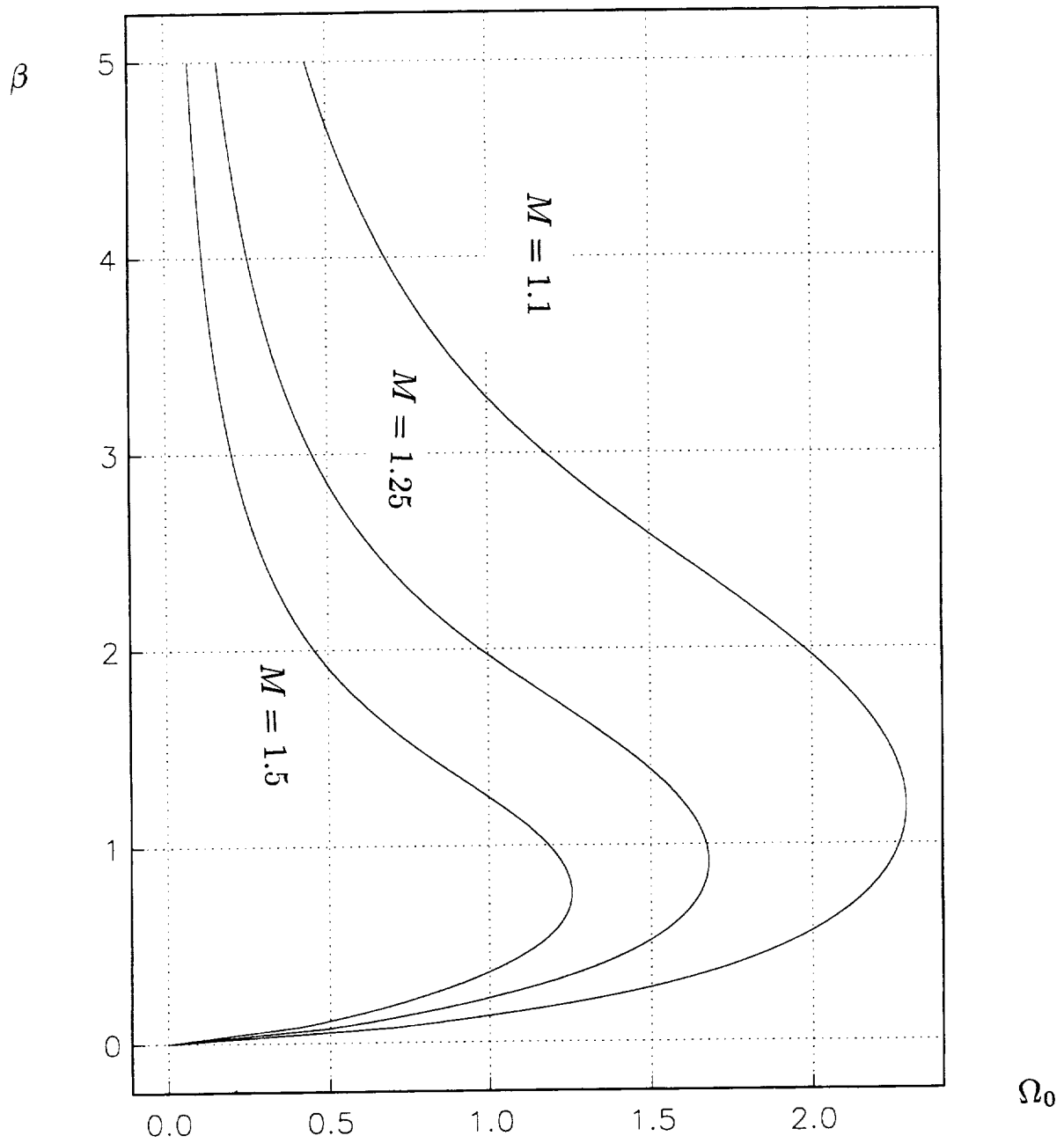
● **Figure 2** The dependence of the neutral linear frequency Ω_0 on the spanwise

Figure 3a, beta=0.1

Figure 3b, beta=0.2

Figure 3c, beta=0.4
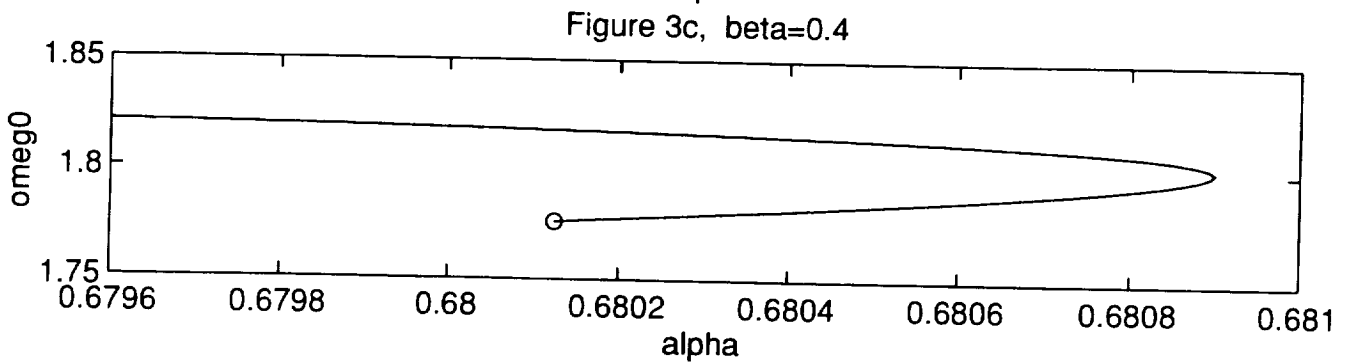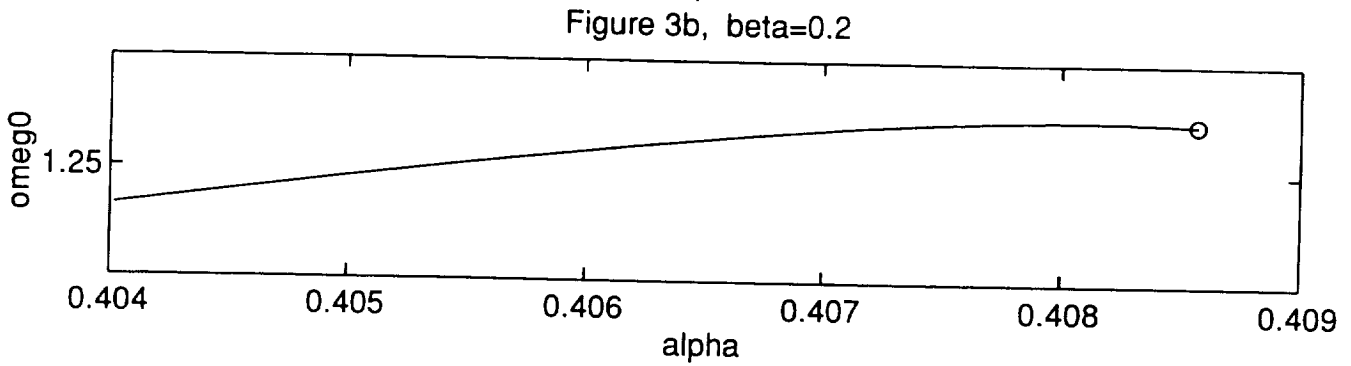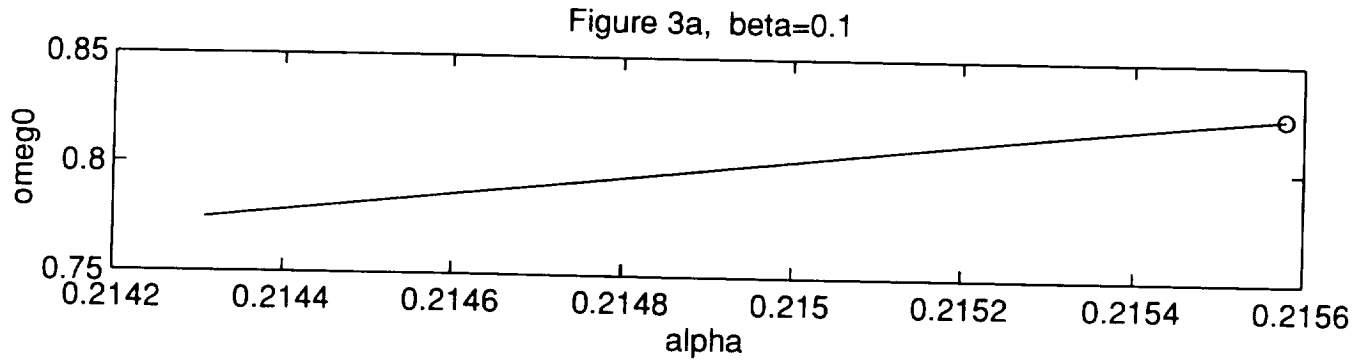
- **Figures 3a-i** The dependence of Ω_0 on α for the nonlinear states with $M_\infty = 1.1$ and $\beta = .1, .2, .4, .6, .8, 1., 1.2, 2.6, 3.0$.

Figure 3d, beta=0.6

Figure 3e, beta=0.8
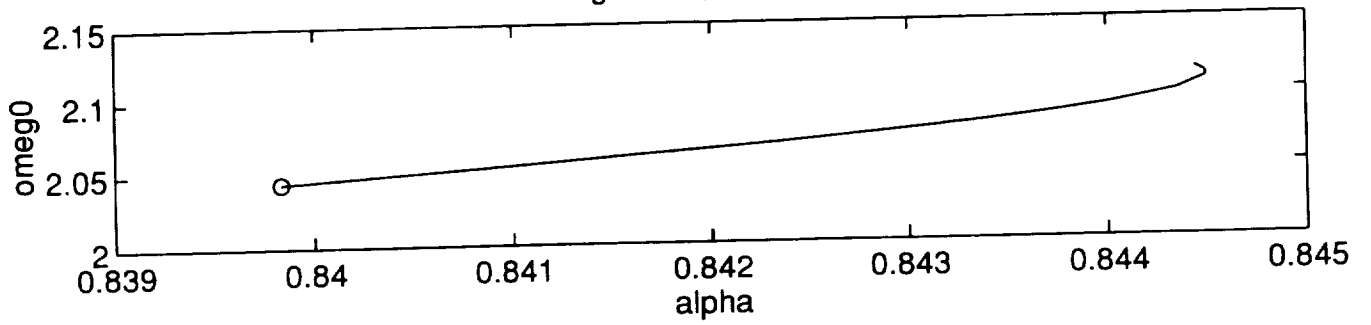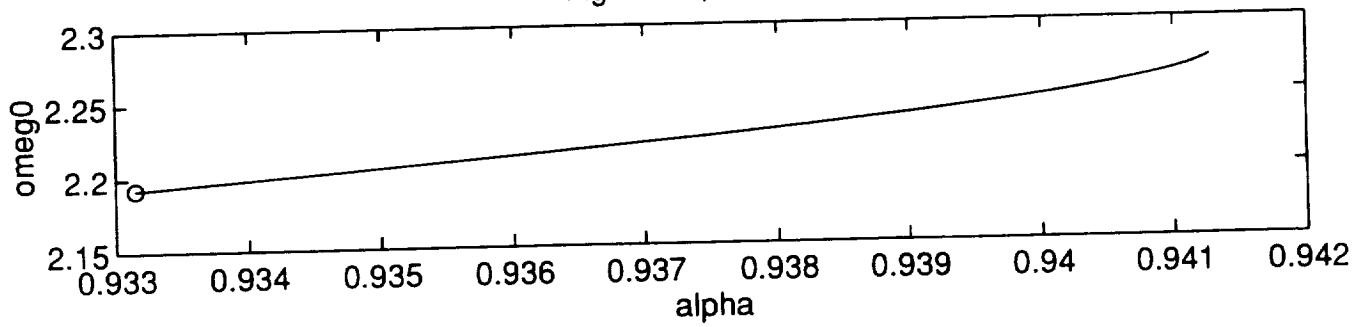
Figure 3f, beta=1.0
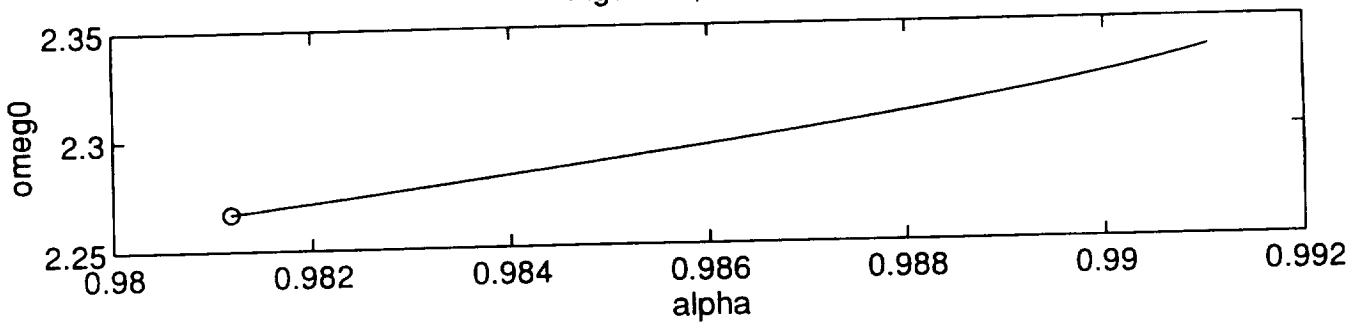
Figure 3g, beta=1.2
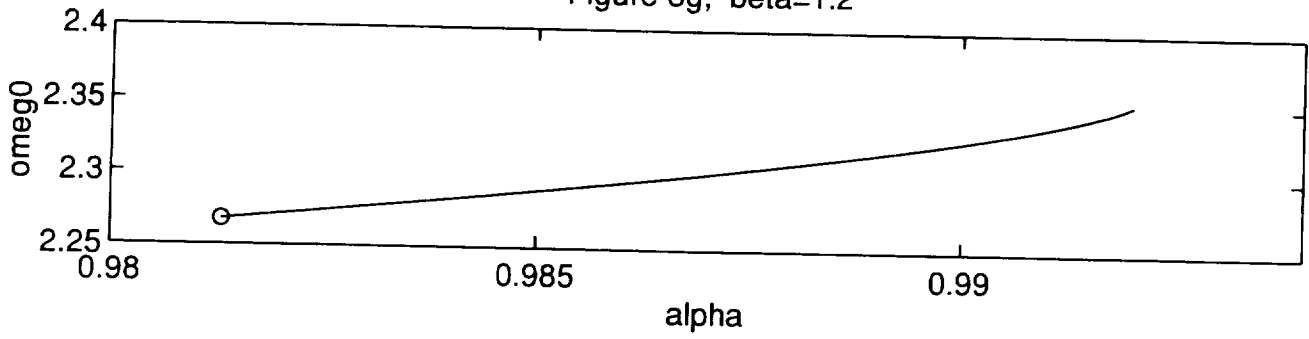
Figure 3h, beta=2.6

Figure 3i, beta=3.0

Figure 4a, beta=0.4

Figure 4b, beta=0.6

Figure 4c, beta=0.8
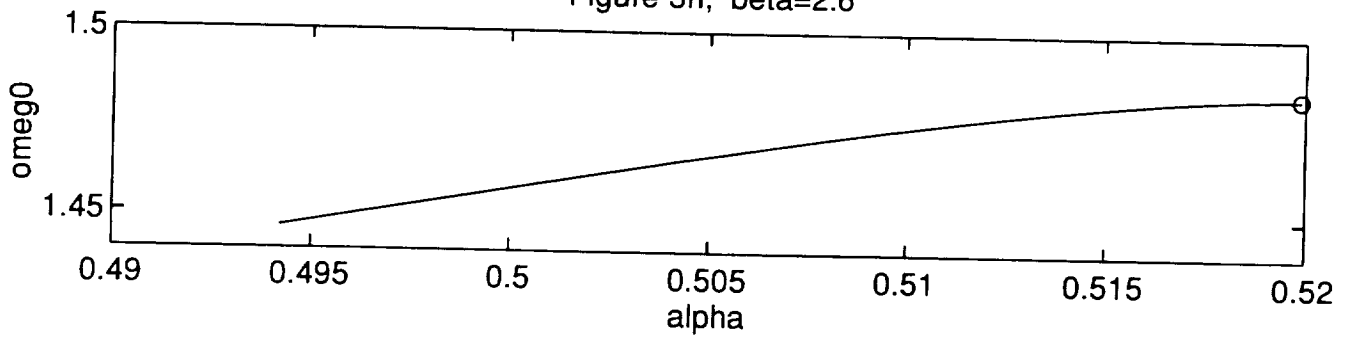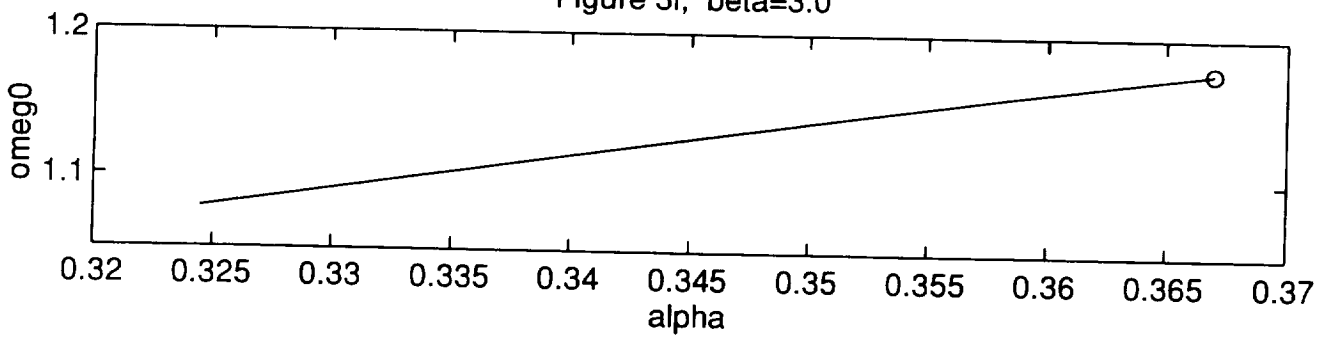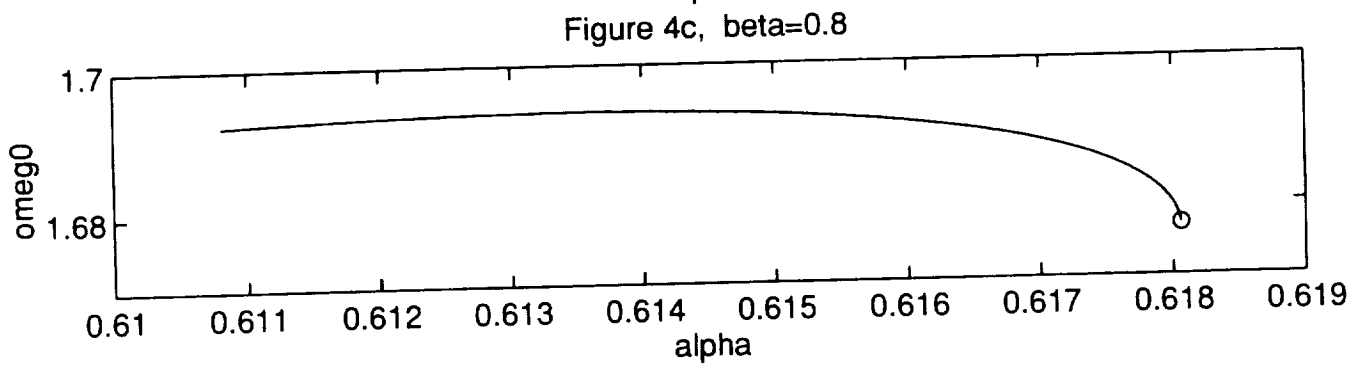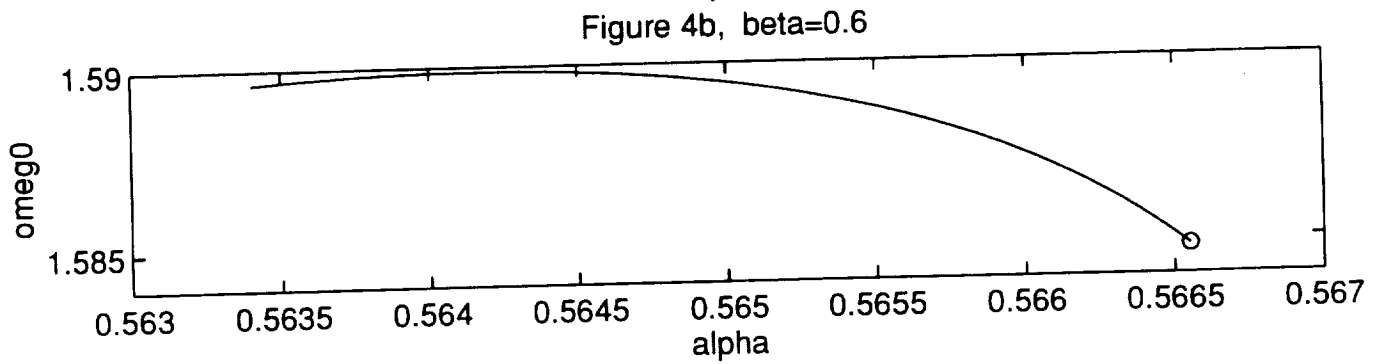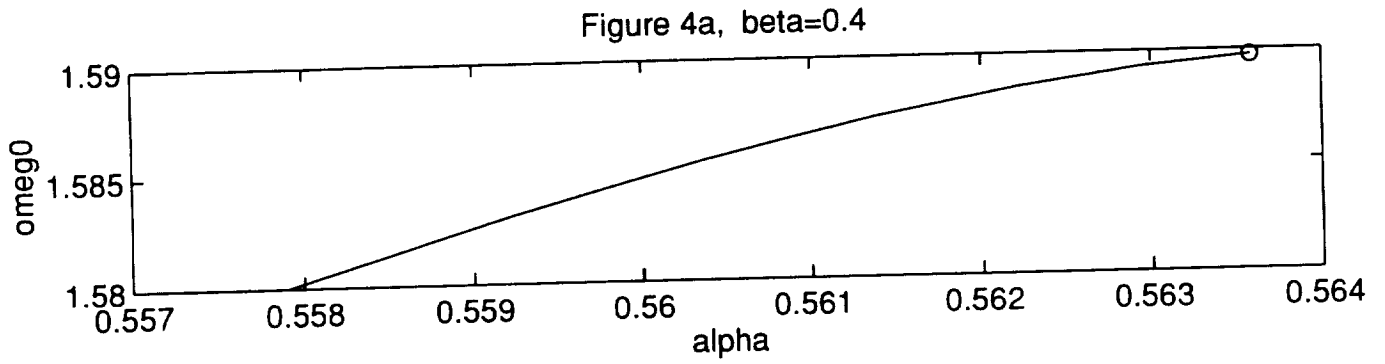
- **Figures 4a-f** The dependence of Ω_0 on α for the nonlinear states with $M_\infty = 1.25$ and $\beta = .4, .6, .8, 1., 1.2, 1.8.$

26

Figure 4d, beta=1.0

Figure 4e, beta=1.2

Figure 4f, beta=1.8

Figure 5a, beta=0.4

Figure 5b, beta=0.6
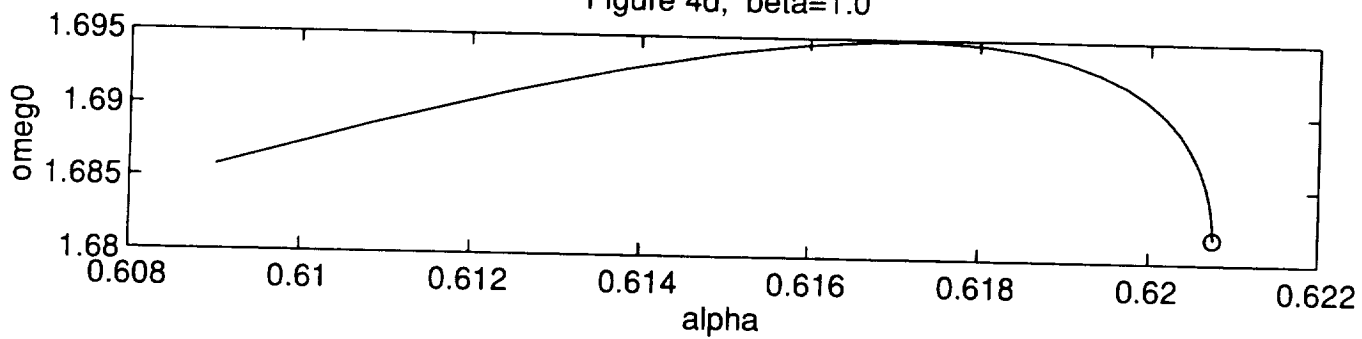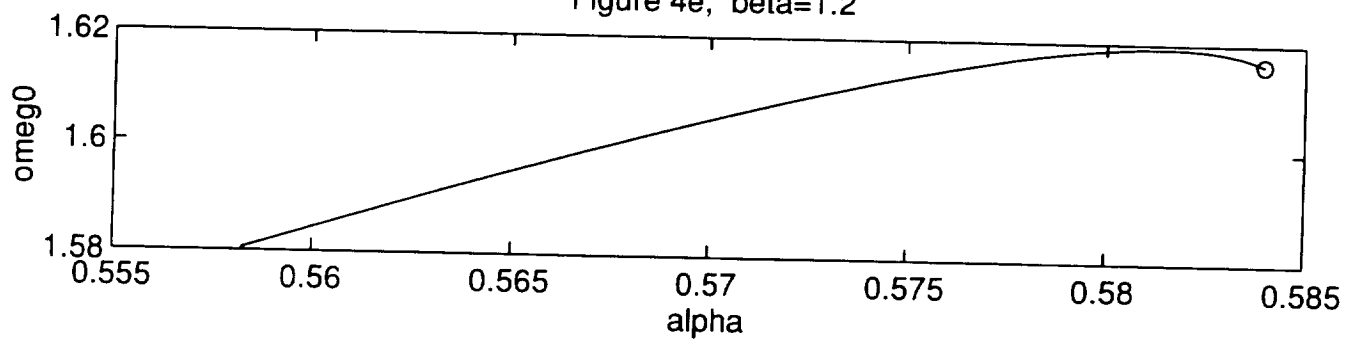
Figure 5c, beta=0.8
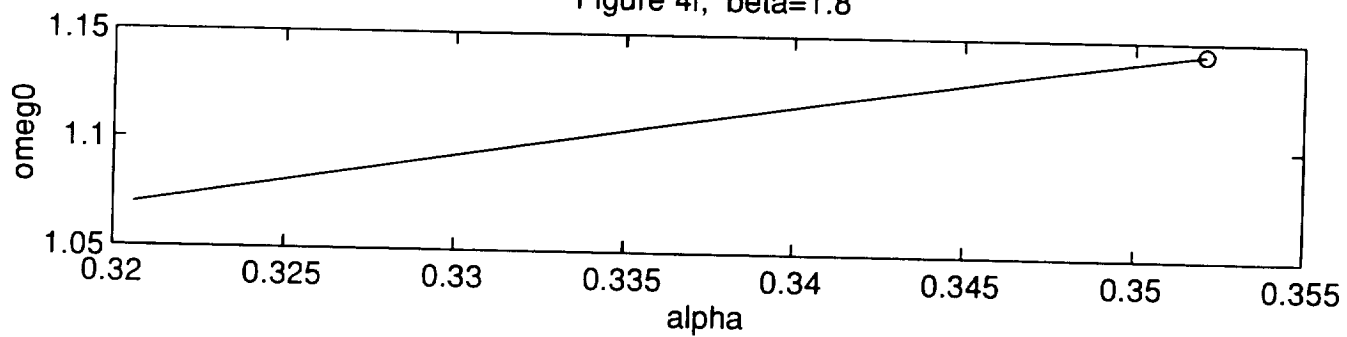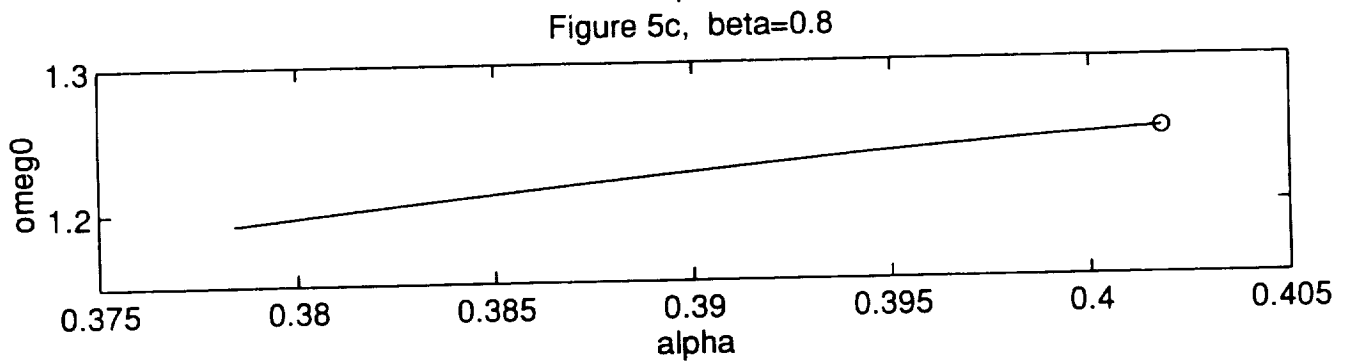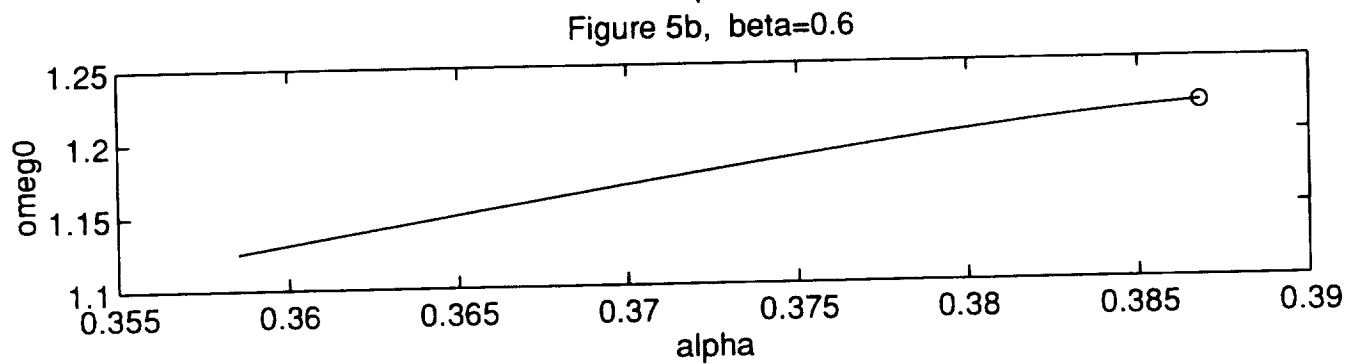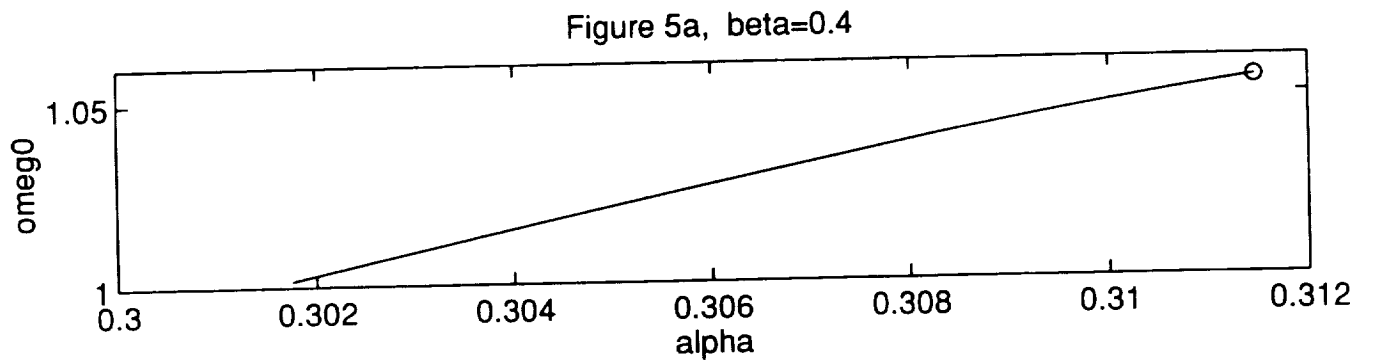
- **Figures 5a-e** The dependence of Ω_0 on α for the nonlinear states with $M_\infty = 1.5$ and $\beta = .4, .6, .8, 1., 1.2$.

Figure 5d, beta=1.0

Figure 5e, beta=1.2
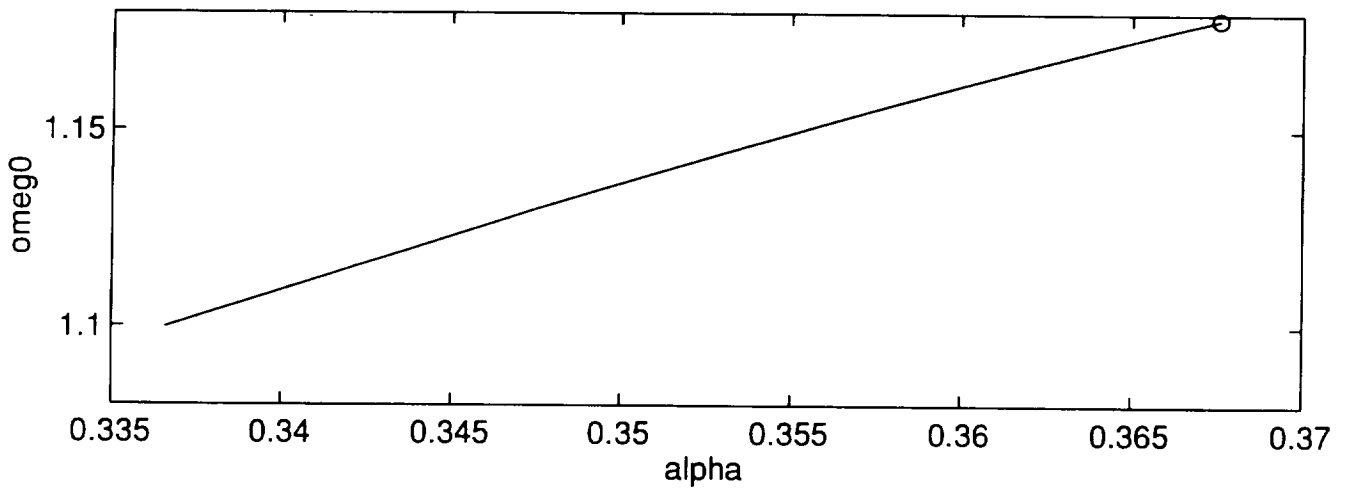
Evolution of u, n=4096, nu=0.1, t=0->1.2
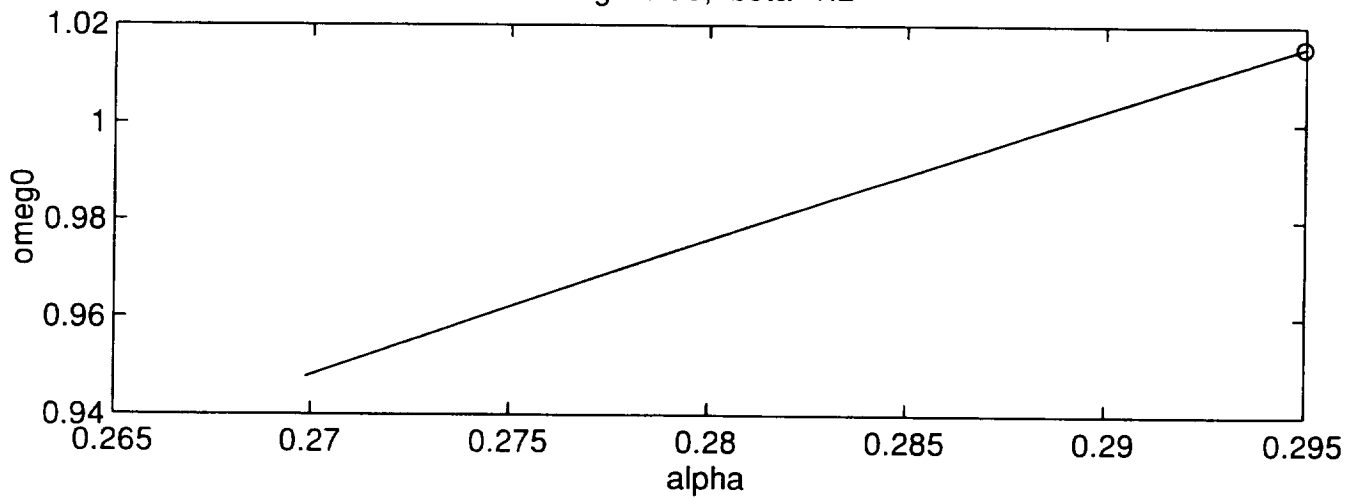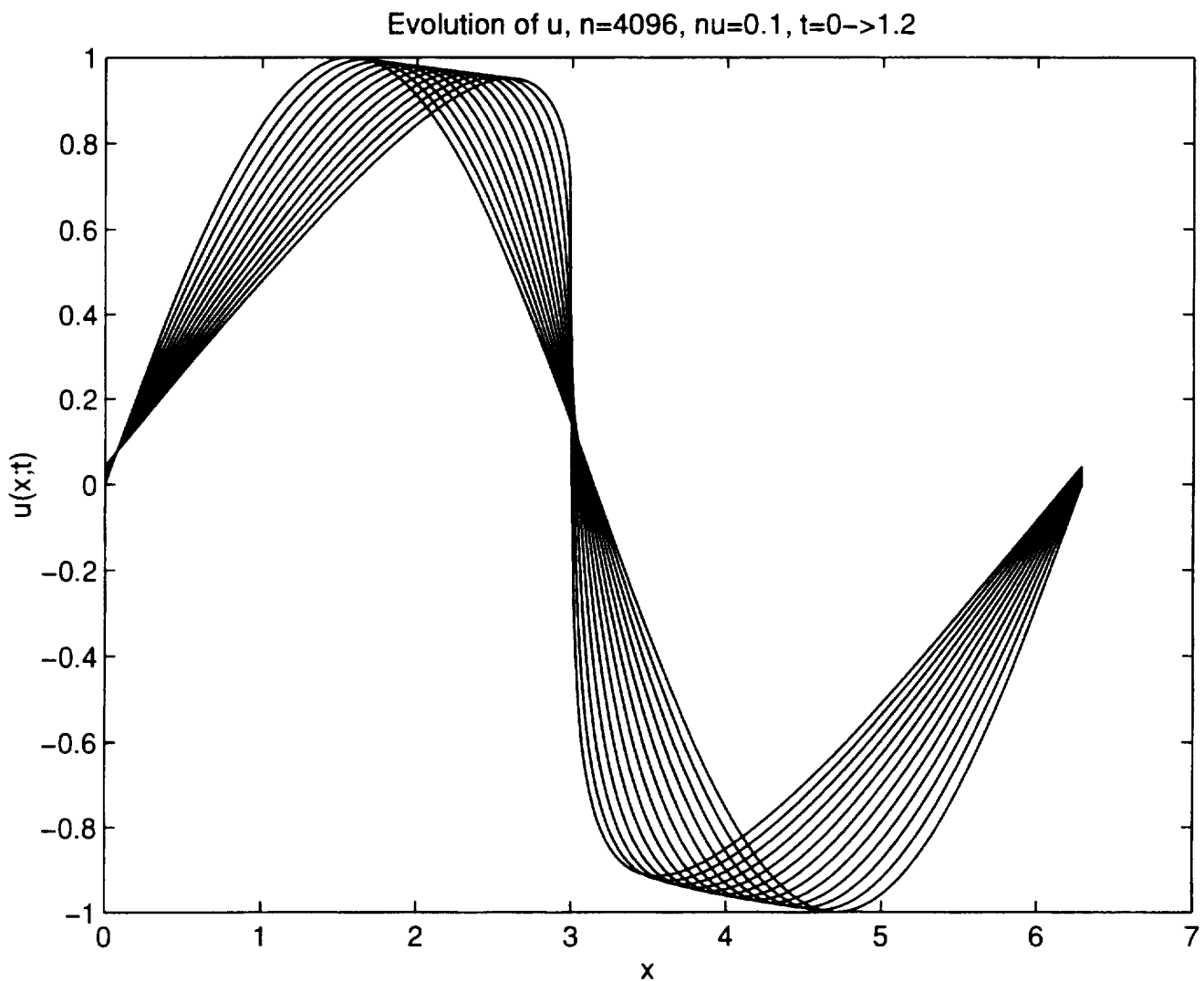
- **Figure 6** (a) Run 1. Evolution of $u(x,t)$: Positive diffusion case $\nu = 0.1$, initial condition $u_0(x) = \sin(x)$, 4096 modes used; profiles shown every 0.1 time units. (b) Final computed profile at $t = 1.246$; minimum slope is -80.03.

Evolution of max slope. n=4096, tfin=1.246, max|u_x|=80.03
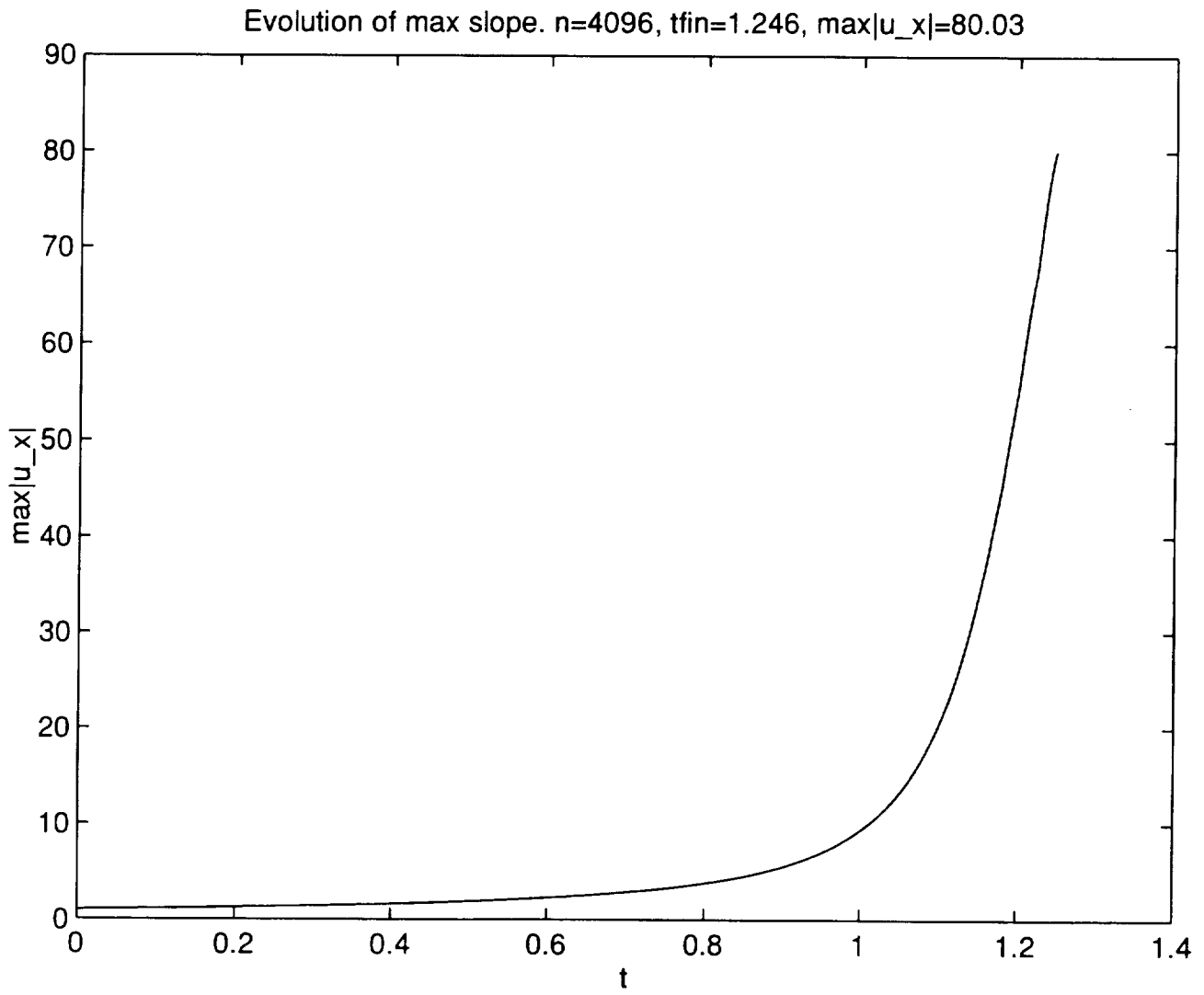
• **Figure 7** Evolution of the maximum of $|u_x|$ for Run 1.

Final computed profile, n=4096, nu=0.1, max|u_x|=80.03, tfin=1.246
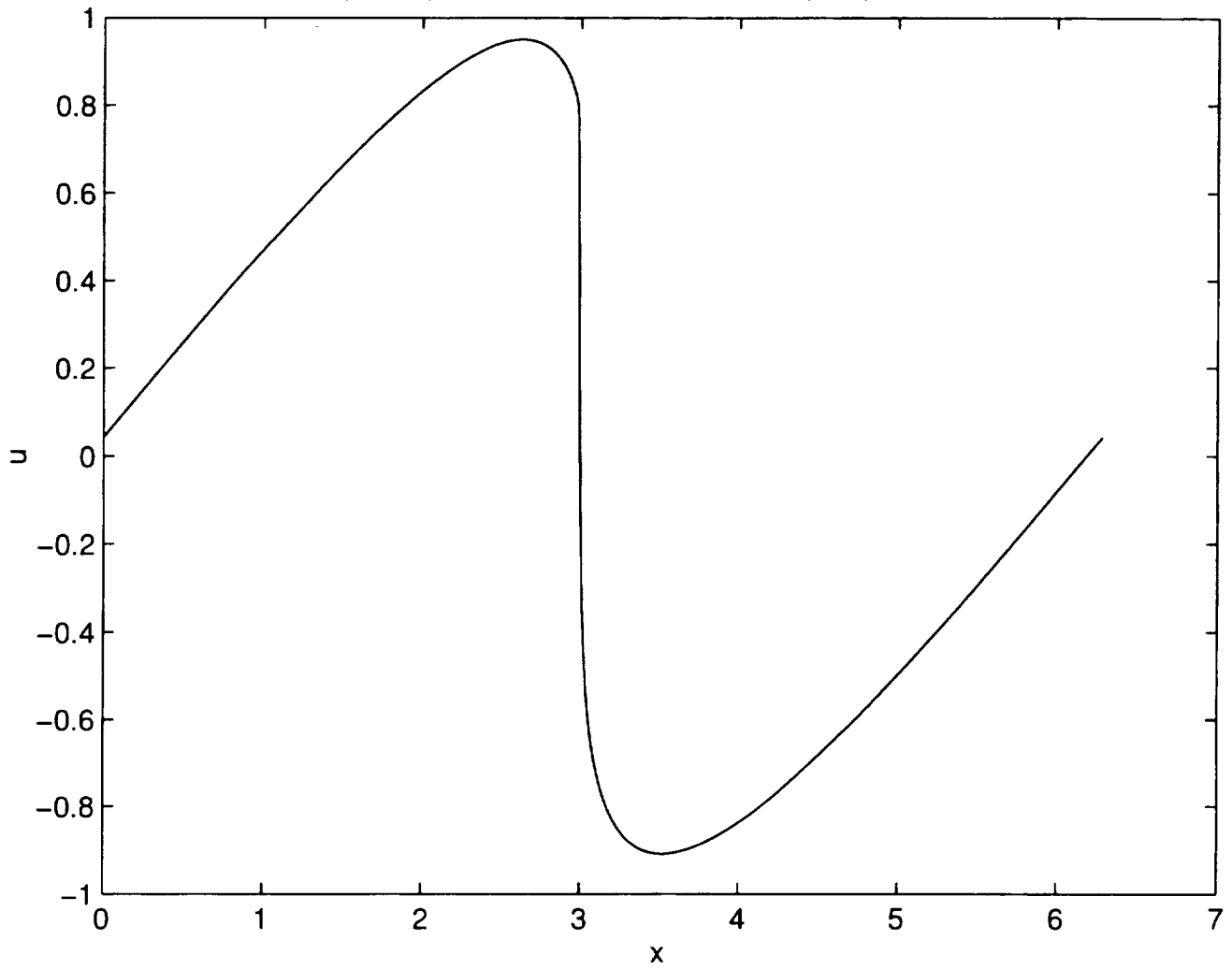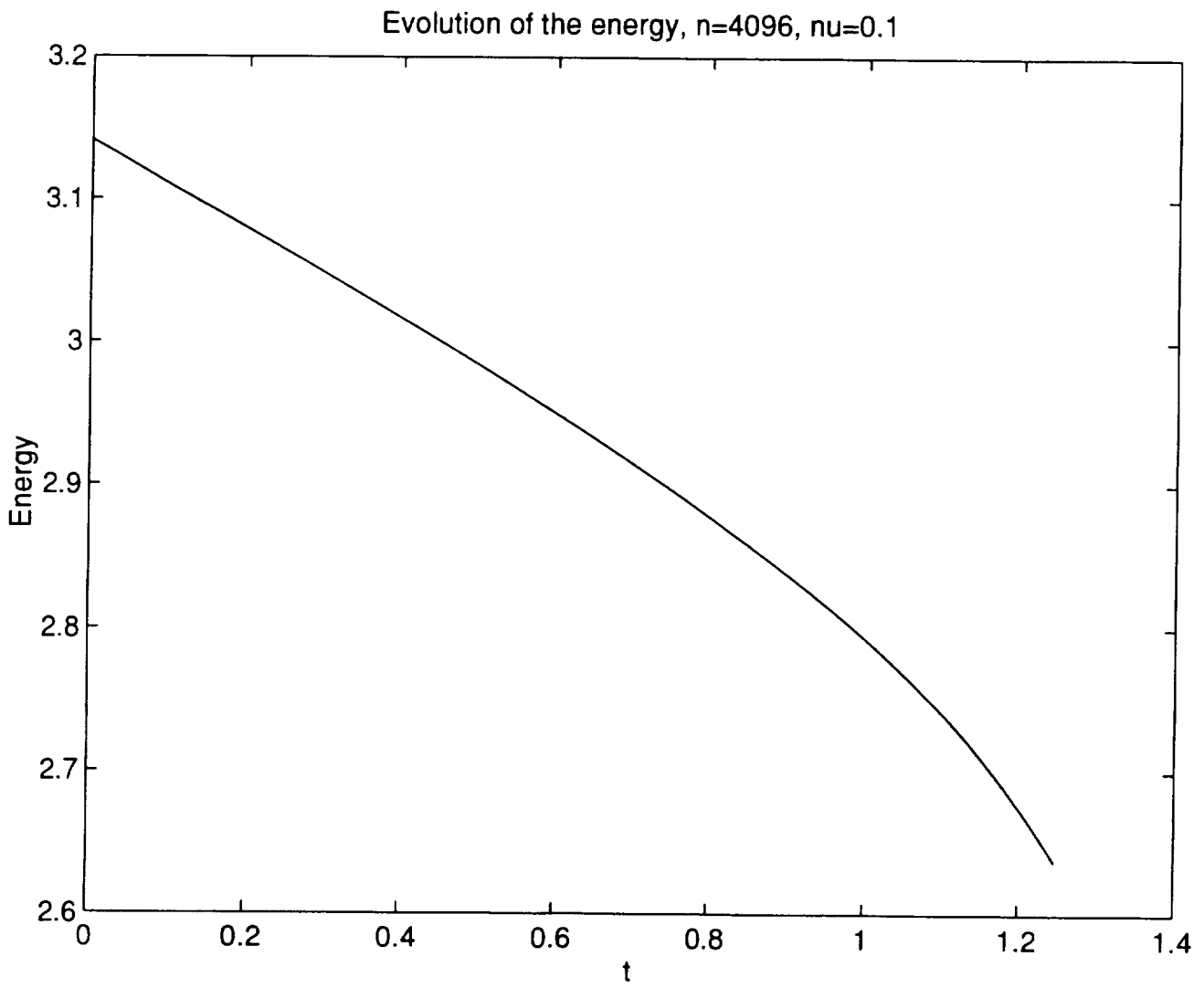
- **Figure 8** Evolution of the energy, $\int_0^{2\pi} u^2(x,t)dx$, for Run 1.

Log–linear evolution of spectral amplitudes, n=4096, nu=0.1, t=0 to 1.246
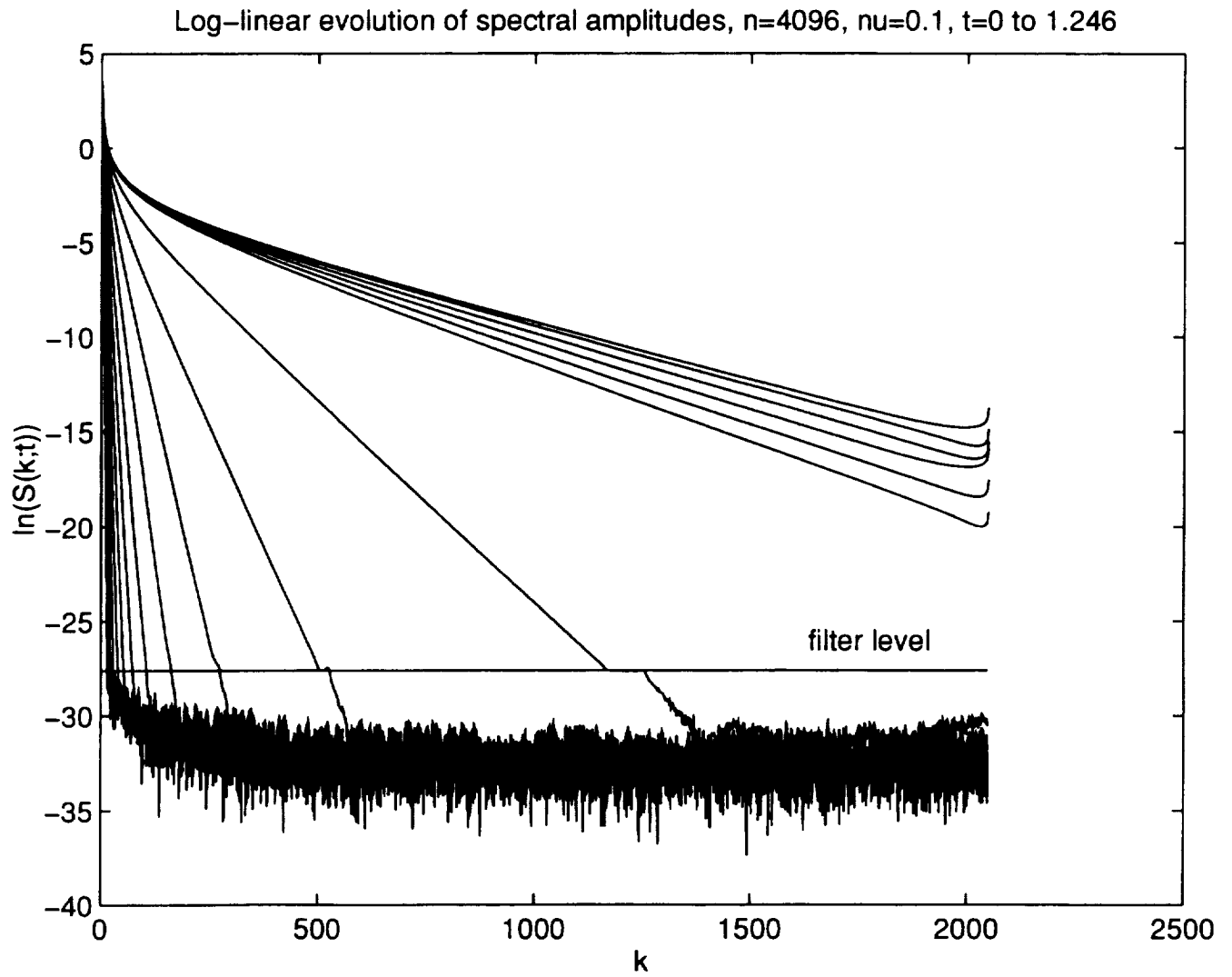
- **Figure 9** Evolution of spectral amplitudes. Log-linear plots corresponding to Run 1. The filter level is set at 10^{-12}.

Log–log evolution of spectral amplitudes, n=4096, nu=0.1, t=0 to 1.246
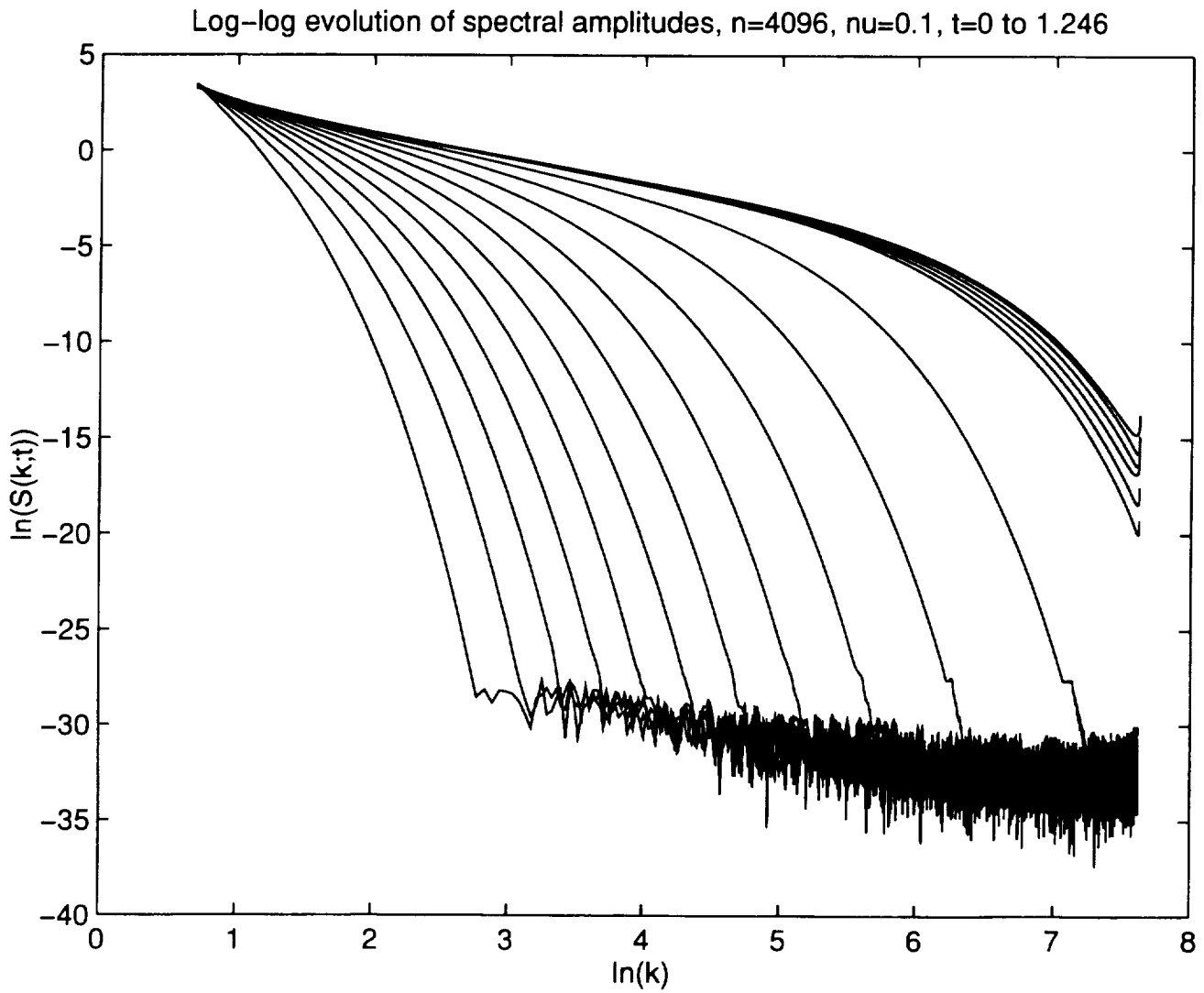
- **Figure 10** Evolution of spectral amplitudes. Log-log plots corresponding to Run 1.

Power law evolution, n=4096, nu=0.1

Evolution of logarithmic decrement, n=4096, nu=0.1
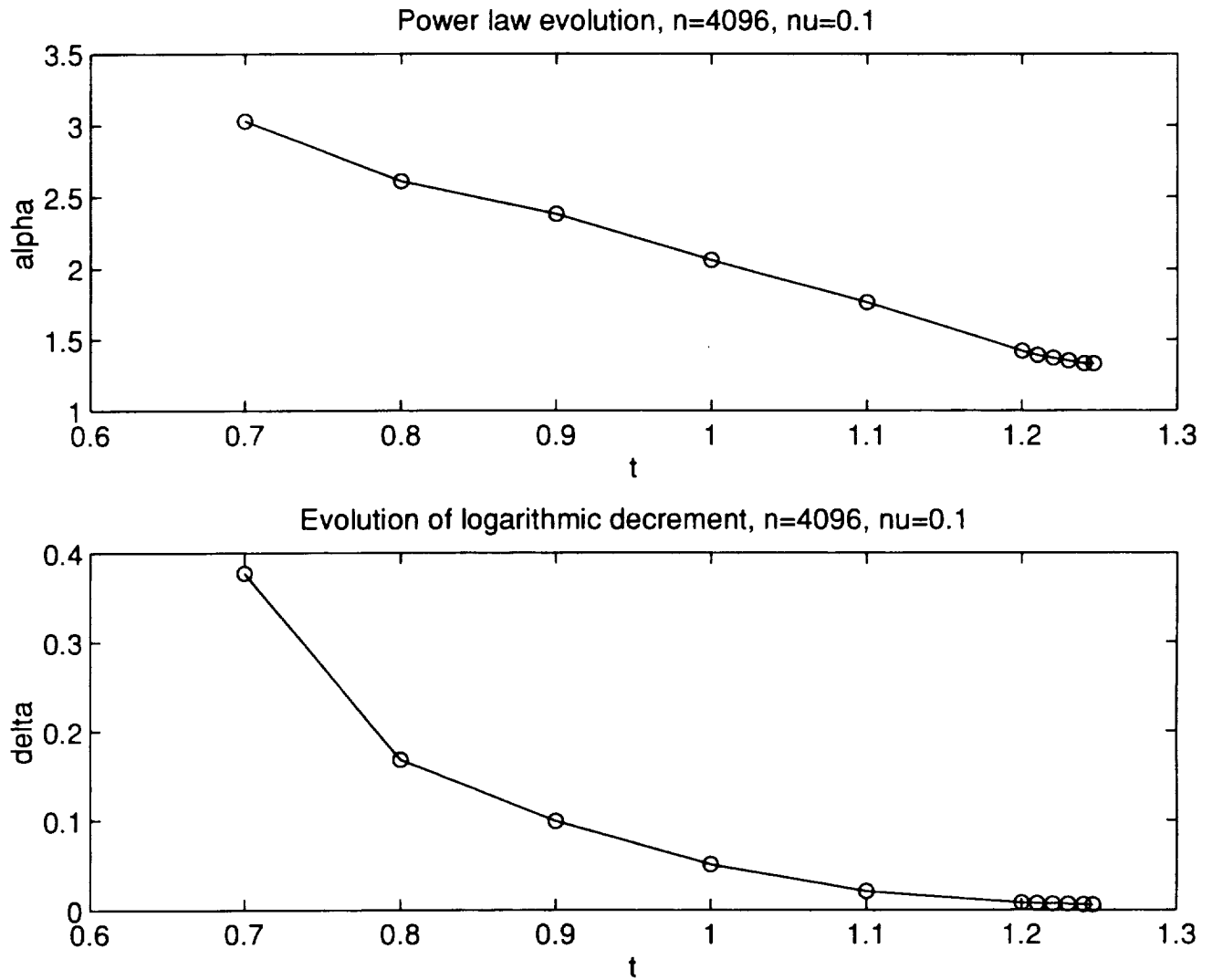
• **Figure 11** (a) Evolution of the power law estimate of the spectrum; (b) evolution of the logarithmic decrement. Both for Run 1.

Evolution of the "enstrophy", n=4096, nu=0.1, tfin=1.246
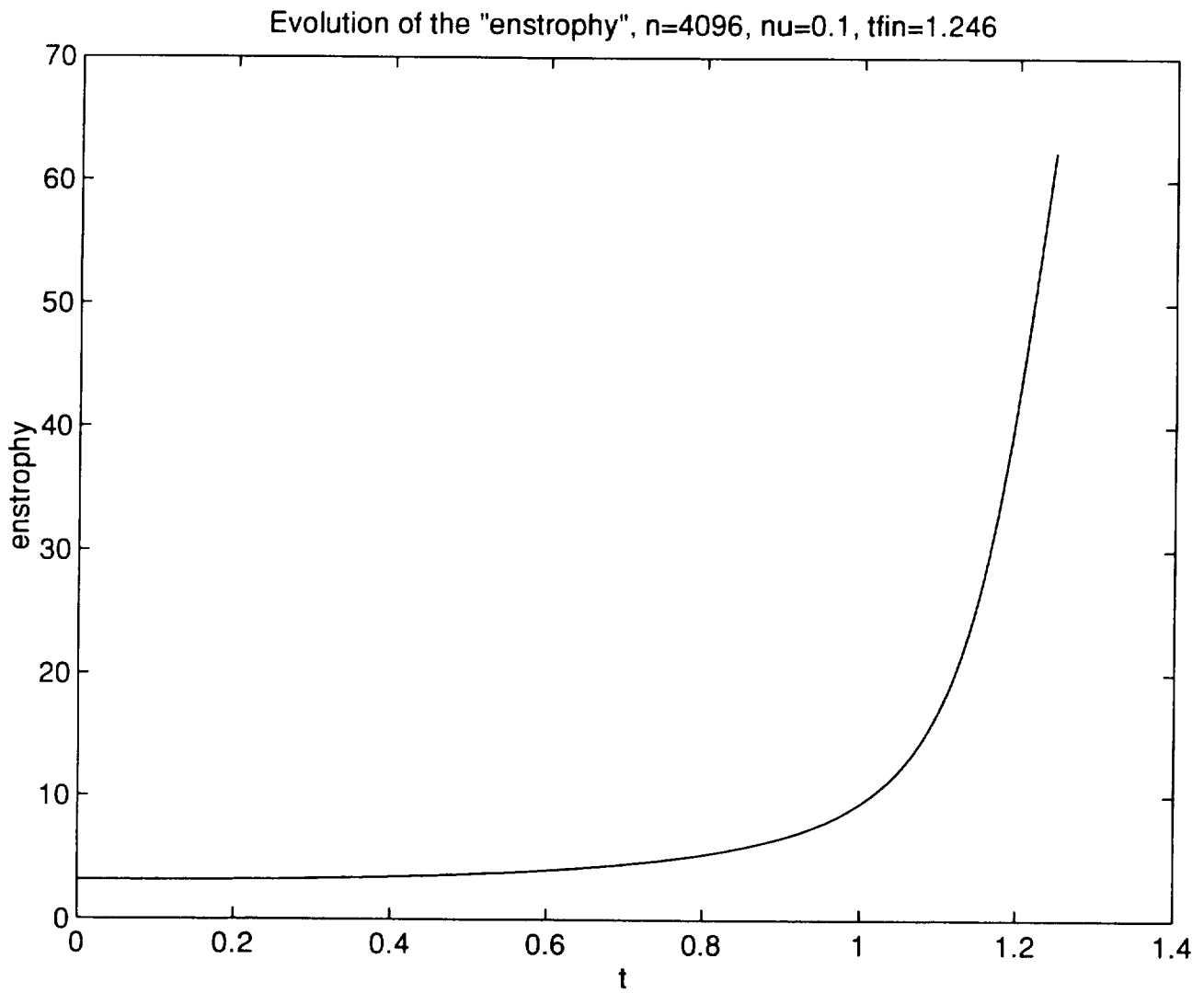
- **Figure 12** Evolution of the enstrophy, $\int_0^{2\pi} u_x^2(x,t)dx$, corresponding to Run 1.

Evolution of u, n=4096, nu=-0.1, t=0-->0.91
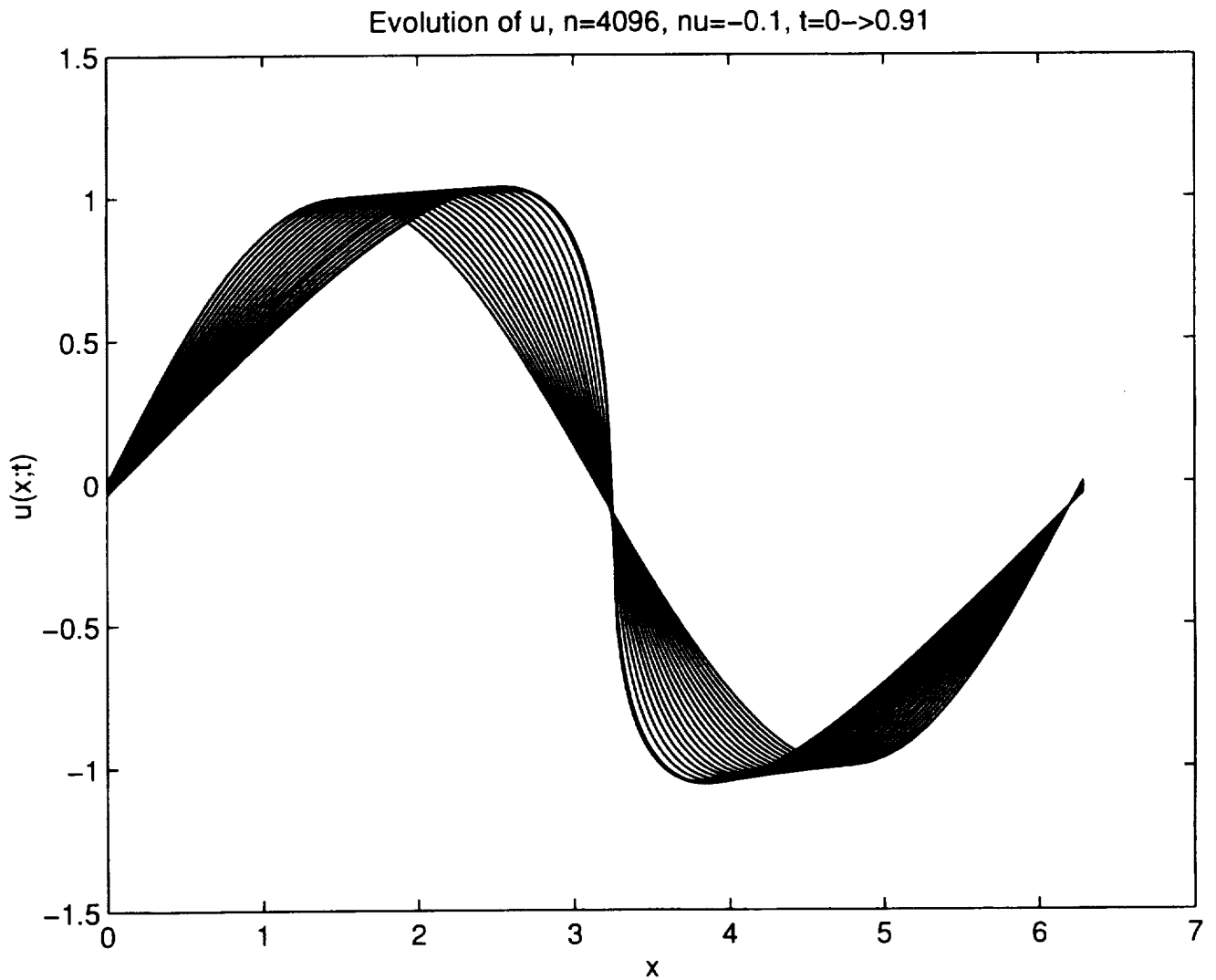
- **Figure 13** Run 2. Evolution of $u(x, t)$: Negative diffusion case $\nu = -0.1$; initial condition obtained by integrating $u_0(x) = \sin(x)$ backwards in time; profiles are plotted every 0.05 time units and the final profile at $t = 0.91$ is also included.
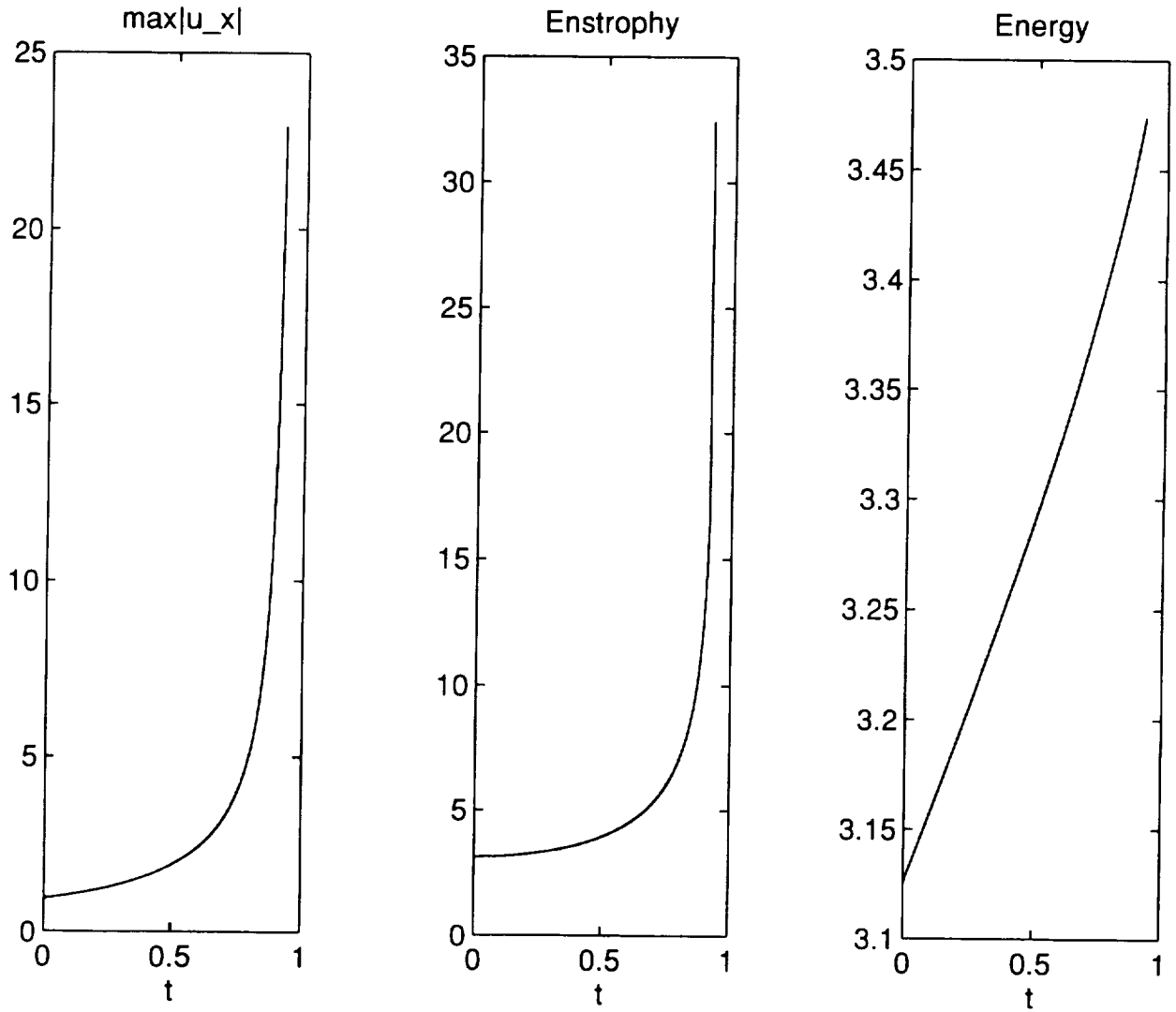
● **Figure 14** Run 2. Evolution with time of (a) $\max|u_x|$, (b) the enstrophy, and, (c) the energy.

Log-linear evolution of spectral amplitudes, n=4096, nu=-0.1, t=0->0.91
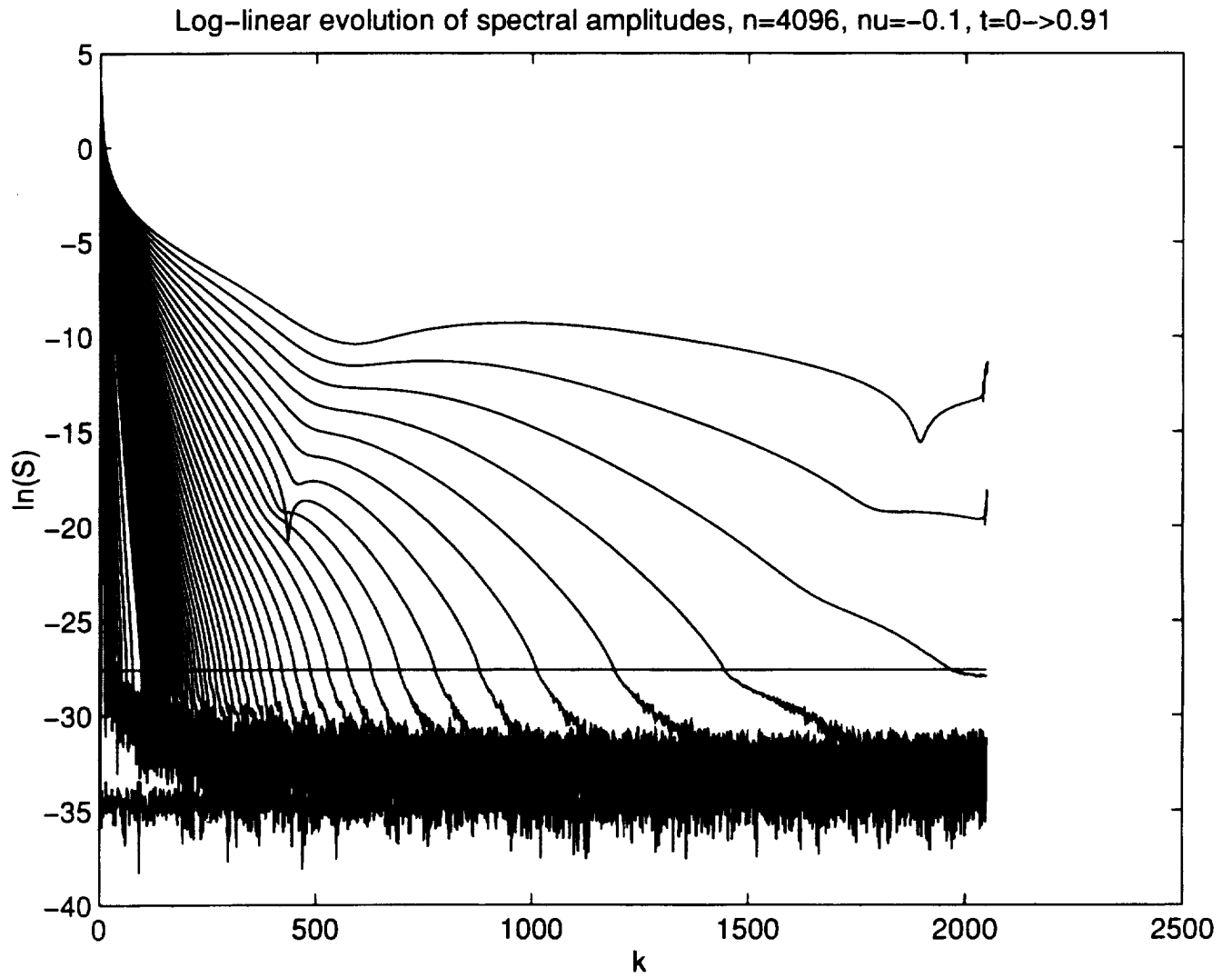
- **Figure 15** Evolution of spectral amplitudes. Log-linear plots corresponding to Run 2. The filter level is set at 10^{-12}.

Log–log evolution of spectral amplitudes, n=4096, nu=−0.1, t=0–>0.91
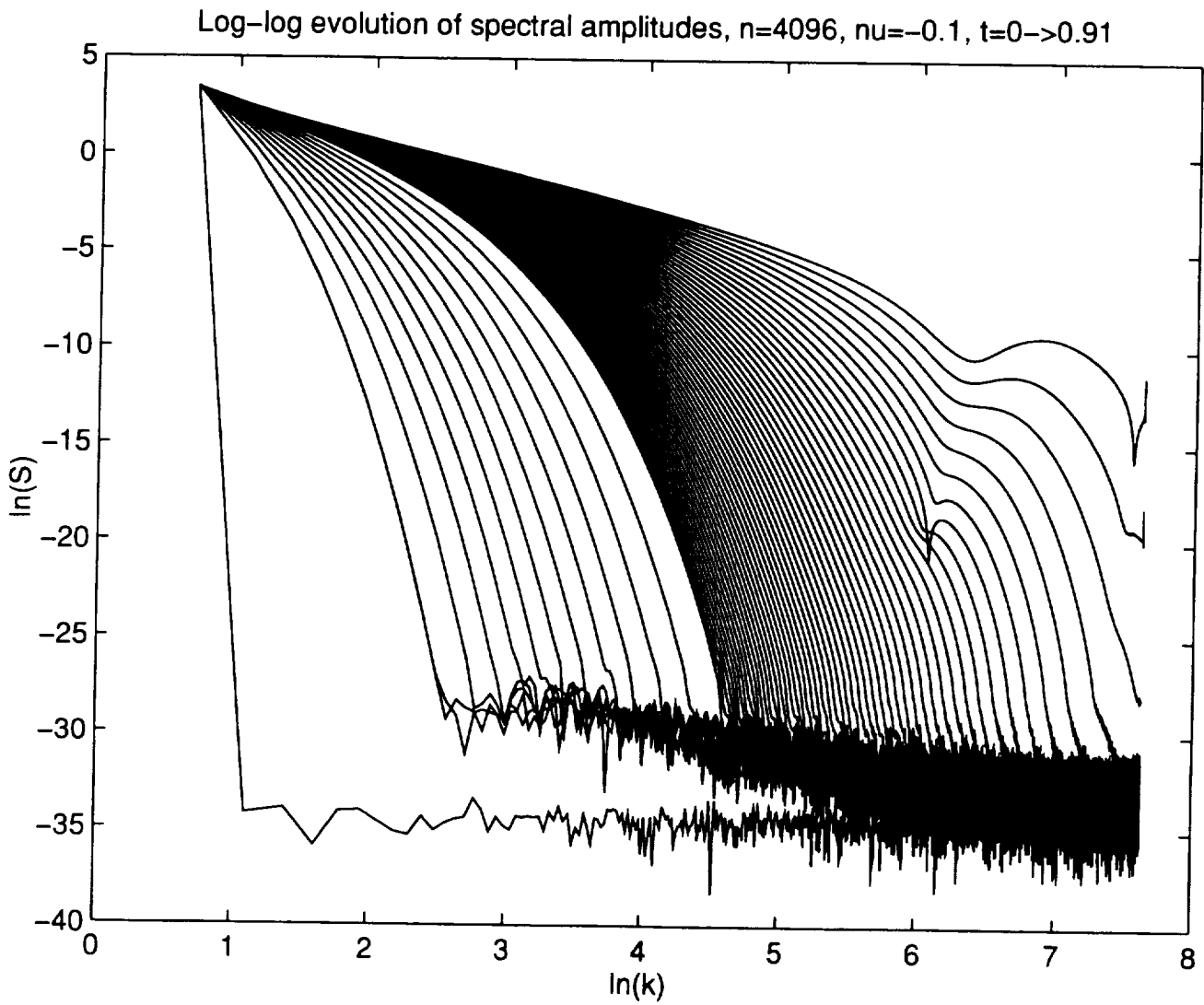
- **Figure 16** Evolution of spectral amplitudes. Log-log plots corresponding to Run 2.

REPORT DOCUMENTATION PAGE

Public reporting burden for this collection of information is estimated to average 1 hour per response, including the time for reviewing instructions, searching existing data sources, gathering and maintaining the data needed, and completing and reviewing the collection of information. Send comments regarding this burden estimate or any other aspect of this collection of information, including suggestions for reducing this burden, to Washington Headquarters Services, Directorate for Information Operations and Reports, 1215 Jefferson Davis Highway, Suite 1204, Arlington, VA 22202-4302, and to the Office of Management and Budget, Paperwork Reduction Project (0704-0188), Washington, DC 20503

1. AGENCY USE ONLY *(Leave blank)*	2. REPORT DATE	3. REPORT TYPE AND DATES COVERED
	April 1995	Contractor Report

4. TITLE AND SUBTITLE
ON THE MODULATIONAL INSTABILITY OF LARGE
AMPLITUDE WAVES IN SUPERSONIC BOUNDARY LAYERS

5. FUNDING NUMBERS
C NAS1-19480
WU 505-90-52-01

6. AUTHOR(S)
Philip Hall
Demetrios T. Papageorgiou

7. PERFORMING ORGANIZATION NAME(S) AND ADDRESS(ES)
Institute for Computer Applications in Science
and Engineering
Mail Stop 132C, NASA Langley Research Center
Hampton, VA 23681-0001

8. PERFORMING ORGANIZATION REPORT NUMBER
ICASE Report No. 95-29

9. SPONSORING/MONITORING AGENCY NAME(S) AND ADDRESS(ES)
National Aeronautics and Space Administration
Langley Research Center
Hampton, VA 23681-0001

10. SPONSORING/MONITORING AGENCY REPORT NUMBER
NASA CR-195072
ICASE Report No. 95-29

11. SUPPLEMENTARY NOTES
Langley Technical Monitor: Dennis M. Bushnell
Final Report
Submitted to SIAM

12a. DISTRIBUTION/AVAILABILITY STATEMENT
Unclassified-Unlimited

Subject Category 34

12b. DISTRIBUTION CODE

13. ABSTRACT *(Maximum 200 words)*
The evolution of large amplitude Tollmien-Schlichting waves in a supersonic boundary layer is investigated. Disturbances which have their wavenumber and frequency slowly varying in time and space are described using a phase equation type of approach. Unlike the incompressible case we find that the initial bifurcation to a finite amplitude Tollmien-Schlichting wave is subcritical for most Mach numbers. In fact the bifurcation is only supercritical for a small range of Mach numbers and even then for only a finite range of wave propagation angles. The modulational instability of large amplitude wavetrains is considered and is shown to be governed by an equation similar to Burgers equation but with the viscous term replaced by a fractional derivative. A numerical investigation of the solution of this equation is described. It is shown that uniform wavetrains are unstable.

14. SUBJECT TERMS
Supersonic; Instability; Modulational

15. NUMBER OF PAGES
44

16. PRICE CODE
A03

17. SECURITY CLASSIFICATION OF REPORT	18. SECURITY CLASSIFICATION OF THIS PAGE	19. SECURITY CLASSIFICATION OF ABSTRACT	20. LIMITATION OF ABSTRACT
Unclassified	Unclassified		